

1 **Variation of the radiative properties during black carbon aging: theoretical**
2 **and experimental intercomparison**

3

4 Cenlin He^{1,2}, Kuo-Nan Liou^{1,2}, Yoshi Takano^{1,2}, Renyi Zhang³, Misti Levy Zamora³, Ping Yang³,
5 Qinbin Li^{1,2}, and L. Ruby Leung⁴

6

7 ¹Department of Atmospheric and Oceanic Sciences, University of California, Los Angeles
8 (UCLA), CA 90095, USA

9 ²Joint Institute for Regional Earth System Science and Engineering, University of California, Los
10 Angeles (UCLA), CA 90095, USA

11 ³Department of Atmospheric Sciences, Texas A&M, College Station, TX 77845, USA

12 ⁴Pacific Northwest National Laboratory, Richland, WA 99352, USA

13

14

15 Correspondence to: Cenlin He (cenlinhe@atmos.ucla.edu)

16

17

18 Abstract

19 A theoretical black carbon (BC) aging model is developed to account for three typical
20 evolution stages, namely, freshly emitted aggregates, coated BC by soluble material, and BC
21 particles undergoing further hygroscopic growth. The geometric-optics surface-wave (GOS)
22 approach is employed to compute the BC single-scattering properties at each aging stage, which
23 are subsequently compared with laboratory measurements. Theoretical calculations are
24 consistent with measurements in extinction and absorption cross sections for fresh BC aggregates
25 with different BC sizes (i.e., mobility diameters of 155, 245, and 320 nm), with differences of \leq
26 25% but overestimate the scattering cross sections for BC mobility diameters of 155, 245, and
27 320 nm, because of uncertainties associated with theoretical calculations for small particles as
28 well as laboratory scattering measurements. The measured optical cross sections for coated BC
29 by sulfuric acid and for those undergoing further hygroscopic growth are generally captured
30 (differences $< 30\%$) by theoretical calculations using a concentric core-shell structure, with
31 differences of less than 20% overestimates in extinction and absorption for the smallest BC size
32 and underestimates in scattering for the largest BC size. This suggests that the core-shell shape
33 represents the realistic BC coating morphology reasonably well in this case, which is consistent
34 with the observed strong structure compaction during aging. We find that the absorption and
35 scattering properties cross sections of fresh BC aggregates vary by 20-40% and 50-65%,
36 respectively, up to 60% due to uncertainty in the BC refractive index the use of upper (1.95 –
37 0.79i) and lower (1.75 – 0.63i) bounds of BC refractive index, which, however, is a factor of two
38 smaller in the case of while the variations are $< 20\%$ in absorption and $< 50\%$ in scattering in the

39 | case of coated BC particles. Sensitivity analyses on the BC morphology show that the optical
40 | properties of fresh BC aggregates are more sensitive to fractal dimension than primary spherule
41 | size. The absorption and scattering cross sections of coated BC particles vary by more than a
42 | factor of two due to different coating structures. We find an increase of 20-250% in absorption
43 | and a factor of 3-15 in scattering during aging, significantly depending on coating morphology
44 | and aging stages. ~~Applying the aging model to CalNex 2010 field measurements, we show that~~
45 | ~~the resulting BC direct radiative forcing (DRF) first increases from 1.5 to 1.7 W m⁻² and~~
46 | ~~subsequently decreases to 1.0 W m⁻² during the transport from the Los Angeles Basin to~~
47 | ~~downwind regions, as a result of the competition between absorption enhancement due to coating~~
48 | ~~and dilution of BC concentration. The BC DRF can vary by up to a factor of two due to~~
49 | ~~differences in BC coating morphology. Thus, This study suggests that~~ an accurate estimate of BC
50 | DRF-radiative effects requires the incorporation of a dynamic BC aging process that accounts for
51 | realistic morphology-coating structures in climate models, ~~particularly for the regional analysis~~
52 | ~~with high atmospheric heterogeneity.~~

53

54 1. Introduction

55 Black carbon (BC) has been identified as the second most important anthropogenic global
56 warming agent in the atmosphere by virtue of its strong absorption of solar radiation and its role
57 as cloud condensation nuclei (CCN) in cloud formation (Ramanathan and Carmichael, 2008;
58 Bond et al., 2013; Wang et al., 2013; Jacobson, 2014). The BC climatic effects are significantly
59 influenced by BC aging process in the atmosphere, which transforms BC from an external to
60 internal mixing state (Schwarz et al., 2008; China et al., 2013) and increases its hygroscopicity
61 (Zhang et al., 2008; Popovicheva et al., 2011) and light absorption (Jacobson, 2001; [Shiraiwa et](#)
62 [al., 2010](#); [Qiu et al., 2012](#); Scarnato et al., 2013).

63 Freshly emitted BC particles are mostly hydrophobic and externally mixed with other
64 aerosol constituents (Zuberi et al., 2005; Zhang et al., 2008). BC agglomerates shortly after
65 emission to form irregular aggregates because of multi-phase processes (Zhang et al., 2008;
66 Pagels et al., 2009; Xue et al., 2009). Early studies have found that BC particles age in the
67 atmosphere through condensation and coagulation processes (e.g., Heintzenberg and Covert,
68 1984; Heintzenberg, 1989). Recent studies confirmed that BC becomes coated by water-soluble
69 material during atmospheric aging, including condensation of sulfate, nitrate, and organics
70 (~~Sehnaiter et al., 2003~~; Moteki et al., 2007; [Shiraiwa et al., 2007](#)), coagulation with preexisting
71 aerosols (Johnson et al., 2005; Kondo et al., 2011), and heterogeneous reactions with gaseous
72 oxidants (Zuberi et al., 2005; Khalizov et al., 2010; Zhang et al., 2012). At the same time, BC
73 aggregates also exhibit considerable restructuring and compaction (Weingartner et al., 1997;
74 Saathoff et al., 2003; Zhang et al., 2008), which significantly alters BC morphology (Adachi and

75 Buseck, 2013; China et al., 2015). Aged BC particles experience hygroscopic growth and
76 activate efficiently as CCN (Zuberi et al., 2005; Zhang et al., 2008). The hygroscopic growth of
77 BC particles depends on its initial size, condensed soluble material mass, surface chemical
78 property, and ambient relative humidity (RH) (Zhang et al., 2008; Khalizov et al., 2009b;
79 Popovicheva et al., 2011).

80 A number of laboratory experiments have been conducted to investigate the effects of
81 atmospheric aging on BC radiative properties. Gangl et al. (2008) showed that internal BC-wax
82 mixture amplifies BC absorption coefficient by ~~a factor of 1.8~~10–90%, depending on the amount
83 of coating. Shiraiwa et al. (2010) found that BC absorption enhancement due to organic coating
84 varies significantly for various BC sizes and coating thickness, with up to a factor of 2
85 enhancement for thick coatings. Under different experimental conditions, relatively small
86 increases (~30%) in BC absorption have also been observed for BC coated by sulfuric acid
87 (Zhang et al., 2008) and some organics (Saathoff et al. 2003). ~~Such significant increase in BC~~
88 ~~absorption has also been observed for BC coated by sulfuric acid (Zhang et al., 2008) and some~~
89 ~~organics (Shiraiwa et al., 2010), while Saathoff et al. (2003) found that organic coating of BC~~
90 ~~particles only increases absorption by 30%.~~ Furthermore, Xue et al. (2009) and Qiu et al. (2012)
91 showed a less than 20% increase in BC absorption for organic coating, which depends on organic
92 species and coating thickness. Thus, the resulting large variation among different experimental
93 studies indicates that the aging effects on BC radiative properties strongly depend on coating
94 material and thickness as well as BC particle size. It is clear, therefore, that experimental details
95 are critically important in making meaningful and appropriate comparisons among various

96 experimental studies involving BC absorption enhancement associated with coating. The
97 disagreement among different laboratory experiments demonstrates large uncertainties associated
98 with BC radiative properties during aging.

99 Field measurements have also revealed substantial variation in BC optical properties during
100 atmospheric aging. Bond and Bergstrom (2006) showed that observed BC mass absorption cross
101 sections (MAC) vary by more than a factor of two (mostly 5-13 m² g⁻¹) under different
102 atmospheric conditions. ~~Schwarz et al. (2008) applied a concentric core shell structure to~~
103 ~~observed coated BC particles using the Mie calculation (Toon and Ackerman, 1981) and found~~
104 ~~that BC coating increases column absorption by 30-50% in the tropical atmosphere. Moffett and~~
105 ~~Prather (2009) measured internally mixed BC particles in Riverside and Mexico City and~~
106 ~~showed that the concentric core shell structure of coated BC results in up to a 60% increase in~~
107 ~~absorption compared with freshly emitted BC. Based on direct measurements at a suburban site~~
108 in Japan, Naoe et al. (2009) showed that coating increases BC absorption by a factor of 1.1-1.4
109 with a larger increase for thicker coatings. Knox et al. (2009) found an absorption enhancement
110 of up to 45% due to BC coating based on measurements in downtown Toronto. Similar increases
111 in absorption have also been directly observed for the internal mixing of biomass-burning BC
112 (Lack et al., 2012). However, Cappa et al. (2012) reported that the observed BC absorption
113 increased only by 6% due to internal mixing based on direct *in situ* during aircraft measurements
114 over California. This implies suggests that BC coating structures coating effects on BC absorption
115 are more rather complex in reality, than the idealized concentric core shell shape which depends
116 on different coating material, mass, and structure influenced by emission sources and

117 [atmospheric processes.](#)

118 Adachi et al. (2010) found that many BC particles embedded within host material are
119 chainlike aggregates locating in off-center positions, based on transmission electron microscope
120 (TEM) observations for samples collected from Mexico City. Using the discrete dipole
121 approximation (DDA) method developed by Draine and Flatau (1994), Adachi et al. showed that
122 a more realistic BC coating morphology results in 20-40% less absorption at visible wavelengths
123 than a concentric core-shell shape. ~~Sedlacek et al. (2012) found that more than 60% of coated BC~~
124 ~~particles have non-core-shell structures in a biomass burning plume. Based on ground-based~~
125 ~~measurements during the California Research at the Nexus of Air Quality and Climate Change~~
126 ~~(CalNex) campaign During the California Research at the Nexus of Air Quality and Climate~~
127 ~~Change (CalNex) 2010 aircraft campaign~~, Adachi and Buseck (2013) further observed that many
128 BC particles are only attached to host material instead of fully embedded within them, leading to
129 only a slight increase in BC absorption. They concluded that the complex mixing structure of BC
130 particles could explain a smaller absorption amplification by BC coating determined from
131 observations than the results computed from an idealized core-shell model. China et al. (2013,
132 2015) classified the observed irregular BC coating shapes into four types: embedded (heavily
133 coated), thinly coated, partly coated, and partially encapsulated. These complex coating
134 structures substantially affect BC optical properties (e.g., Videen et al., 1994; Liu and
135 Mishchenko, 2007; Kahnert et al., 2013), which is one of the most important uncertainty sources
136 in evaluating BC direct radiative forcing (DRF) (Bond et al., 2013). Thus, a reliable estimate of
137 BC DRF requires a quantitative understanding of the evolution of BC radiative properties under

138 the influence of various morphology during atmospheric aging.

139 In this study, we have developed a theoretical BC aging model based on the current
140 understanding of BC aging process, which accounts for three major stages, namely, freshly
141 emitted aggregates, coated BC by soluble material, and BC particles undergoing further
142 hygroscopic growth. We apply the geometric-optics surface-wave (GOS) approach to compute
143 light absorption and scattering of BC particles at each aging stage. The theoretical calculations
144 are compared with laboratory measurements, followed by a systematic evaluation of
145 uncertainties associated with BC morphology and refractive index. ~~We further apply the aging
146 model to the CalNex 2010 field campaign to evaluate the evolution of BC DRF over southern
147 California by coupling with a radiative transfer model (RTM) for analysis.~~ Finally, we discuss
148 the implication of model results for BC ~~DRF~~radiative effect assessment.

149

150 2. Methods

151 2.1 A theoretical BC aging model

152 Based on the current knowledge of BC atmospheric aging, we have developed a theoretical
153 model accounting for three major BC aging stages, as depicted in Fig. 1. Stage I represents
154 freshly emitted BC aggregates that are externally mixed with other particles. Stage II represents
155 BC particles coated by water-soluble aerosol constituents through condensation, coagulation,
156 and/or heterogeneous oxidations. Stage III represents BC particles coated by both soluble
157 material and water through hygroscopic growth. ~~In this study, According to atmospheric
158 observations,~~ six typical BC coating structures (Fig. 1) have been considered for Stages II and

159 III to approximately represent observations in the real atmosphere or laboratory in this study (Fig.
160 4), including embedded (i.e., concentric core-cell, off-center core-shell, and closed-cell), partially
161 encapsulated, and partly coated (i.e., open-cell and externally attached) structures following the
162 classification presented in China et al. (2013, 2015). The concentric and off-center core-shell
163 structures (Martin et al., 1998; Sedlacek et al., 2012) are a result of considerable collapse of BC
164 aggregates into more compact and spherical clusters when fully engulfed in coating material
165 (Zhang et al., 2008). The closed-cell structure is an example where coating material not only
166 covers the outer layers of BC aggregates but also fills the internal voids among primary
167 spherules (Strawa et al., 1999). The partially encapsulated structure is formed when only a part
168 of BC aggregate merges inside coating material (China et al., 2015). The open-cell and externally
169 attached structures are produced by coating material sticking to a part of BC aggregates' surface
170 (Stratmann et al., 2010; China et al., 2015). We wish to note that the six coating structures used
171 in this study, including closed-cell and open-cell structures, are theoretical models and as such,
172 they may not completely capture detailed BC coating structures from aircraft and ground-based
173 observations. Further hygroscopic growth of BC particles after Stage III could lead to the
174 formation of cloud droplets, a subject beyond the scope of the present study.

175

176 **2.2 Laboratory measurements**

177 The physical and radiative properties of BC particles during aging after exposure to sulfuric
178 acid (H₂SO₄) under various RH conditions (5-80%) have been measured in the laboratory by
179 Zhang et al. (2008) and Khalizov et al. (2009a). BC aggregates were generated by incomplete

180 combustion of propane in a laminar diffusion burner (Santoro et al., 1983) and sampled by a
181 pinhole diluter (Kasper et al., 1997). A tandem differential mobility analyzer (TDMA) system
182 was used to produce singly-charged mobility-classified BC particles, followed by a coating
183 chamber with controlled RH and H₂SO₄ vapor concentrations at room temperatures (299±1 K).
184 The BC mass and size growth due to H₂SO₄ and water vapor (H₂O) condensation during aging
185 were measured by an aerosol particle mass (APM) analyzer and TDMA, respectively. The
186 effective density and fractal dimension (D_f) of BC particles were derived from the measured BC
187 mobility diameter (D_{BC}) and mass (see Eqs. 1 and 2 in Zhang et al., 2008). The compaction and
188 restructuring of BC aggregates were captured by a TEM (see Fig.1 in Zhang et al., 2008). BC
189 extinction and scattering cross sections were measured at 532-nm wavelength by a cavity
190 ring-down spectrometer (CRDS) and an integrating nephelometer, respectively. The absorption
191 cross section was determined from the resulting difference between extinction and scattering
192 cross sections. Khalizov et al. (2009a) showed that ~~the experimental uncertainties~~ uncertainty
193 associated with in measured optical cross sections of coated BC particles is within 10%, which
194 primarily represents uncertainty in relative humidity, particle size, number density, and
195 instrument calibration. ~~instrument calibration, relative humidity, and particle size measurements~~
196 ~~were within 10%, which~~ This uncertainty, however, excludes ~~does not include~~ the contribution
197 from multiply charged particles, ~~while the scattering measurements of freshly emitted BC~~
198 ~~aggregates were associated with high uncertainty.~~ For freshly emitted BC aggregates, measured
199 scattering cross sections involve relatively large uncertainties. More details in laboratory
200 experiments have been presented in Zhang et al. (2008) and Khalizov et al. (2009a). Three

201 experimental cases with initial D_{BC} of 155, 245, and 320 nm were used in this study (see Table 1).

202 In each case, BC particles exposed to H_2SO_4 vapor (1.4×10^{10} molecules cm^{-3}) at 5% and 80%

203 RH were used to represent coated BC at Stages II and III (see Sect. 2.1), respectively.

204

205 **2.3 Geometric-optics surface-wave (GOS) approach**

206 We employed the GOS approach developed by Liou et al. (2011, 2014), which explicitly

207 treats fractal aggregates and various coating structures, to compute absorption and scattering

208 properties of BC particles at three aging stages. In the GOS approach, a stochastic procedure

209 developed by Liou et al. (2011) is applied to simulate homogeneous aggregates and coated

210 particles with different shapes in a 3-D coordinate system. In this study, we have extended the

211 original stochastic process to generate more complex coating morphology, including the partially

212 encapsulated and externally attached structures (see Figs. S1-S6 in the supplementary material).

213 Once the particle shape and composition are determined by the stochastic procedure, the

214 reflection and refraction of particles are computed with the hit-and-miss Monte Carlo photon

215 tracing technique. The extinction and absorption cross sections are derived following a

216 ray-by-ray integration approach (Yang and Liou, 1997). Diffraction by randomly oriented

217 nonspherical particles is computed on the basis of Babinet's principle ([Born and Wolf, 1999](#)) and

218 photon-number weighted geometric cross sections. The GOS approach accounts for the

219 interaction of incident waves at grazing angles near the particle edge and propagating along the

220 particle surface into shadow regions, referred to as the surface wave, using the formulation

221 developed by Nussenzweig and Wiscombe (1980) for spheres as the basis for physical

222 adjustments and application to nonspherical particles (Liou et al., 2010, 2011). The concept of
223 the GOS approach is graphically displayed in Fig. 2 and it is designed for computations of
224 absorption and extinction cross sections and asymmetry factors in line with experimental results.

225 Liou et al. (2010, 2011) and Takano et al. (2013) demonstrated that the single-scattering
226 properties of aerosols with different sizes and shapes determined from the GOS approach
227 compare reasonably well (differences < 20%) with those determined from the Finite Difference
228 Time Domain (FDTD) method (Yang and Liou, 1996) and DDA (Draine and Flatau, 1994) for
229 column and plate ice crystals, the superposition T-matrix method (Mackowski and Mishchenko,
230 1996) for fractal aggregates, and the Lorenz-Mie model (Toon and Ackerman, 1981) for a
231 concentric core-shell shape. Moreover, compared with other numerical methods, the GOS
232 approach can be applied to a wider range of particle sizes, shapes, and coating morphology with
233 a high computational efficiency, including very large particles (e.g., ~100-1000 μm snowflakes)
234 and complex multiple inclusions of aerosols within irregular snow grains (Liou et al., 2014; He
235 et al., 2014), in which the FDTD, DDA, and T-matrix methods have not been able to apply. As
236 stated previously, the GOS approach has been developed specifically for ~~extinction and~~
237 ~~absorption~~optical cross sections (i.e., extinction, absorption, and scattering) and the asymmetry
238 factor, ~~but not for scattering phase matrix calculations~~. Also, due to the approximation in the use
239 of geometric photon tracing, the GOS approach has limitation and uncertainty for application to
240 size parameters much smaller than 1. To supplement GOS, we have developed the
241 Rayleigh-Gan-Debye (RGD) approximation coupled with GOS for very small particles, which
242 has been cross-validated with the superposition T-matrix method (Takano et al., 2013). Takano et

243 al. (2013) showed that the coupled GOS-RGD and superposition T-matrix results are both close
244 to the observed specific absorption of BC aggregates for the range of size parameter considered
245 in the present study. (Takano et al., 2013). The ~~combined-coupled~~ GOS/RGD approach can be
246 applied to size parameters covering 0.1 to 1000. In the present study, the coupled GOS-RGD
247 approach is used for fresh BC aggregates (Stage I), while the GOS approach without RGD
248 coupling is used for coated BC particles (Stages II and III).

249

250 **2.4 Theoretical calculations**

251 We used BC physical properties measured from laboratory experiments (see Sect. 2.2) as
252 input to theoretical calculations (see Table 1). In standard calculations, the freshly emitted BC
253 aggregates (Stage I) were assumed to be comprised of primary spherules with a diameter of 15
254 nm measured from the experiments and were constructed by the GOS stochastic procedure to
255 reproduce the measured mass and fractal dimension (= 2.1) of BC aggregates. The BC mass was
256 the product of measured BC effective densities and mobility volumes. The mass of H₂SO₄
257 coating on BC at Stage II was derived from the observed relationship between condensed H₂SO₄
258 mass and particle diameter at 5% RH. The mass of H₂O condensed on H₂SO₄-coated BC at Stage
259 III was derived from the measured hygroscopic mass growth ratio of H₂SO₄-coated BC at 80%
260 RH. In standard calculations, we used a concentric core-shell structure for coated BC particles at
261 Stages II and III because of the strong particle compaction during aging based on laboratory
262 observations (Zhang et al., 2008). Thus, BC core size and coating thickness were computed from
263 the mass of BC and H₂SO₄/H₂O coating. The refractive index (RI) of H₂SO₄-H₂O coating at

264 Stage III was derived as the volume-weighted RI of H₂SO₄ and H₂O. We used a BC RI of 1.95 -
265 0.79i (upper bound) recommended by Bond and Bergstrom (2006) and a BC density of 1.77 g
266 cm⁻³ suggested by Zhang et al. (2008). Under the preceding conditions, computations of BC
267 optical properties at 532-nm wavelength were carried out for comparison with laboratory
268 measurements. The comparison between GOS and experimental results in this study provides an
269 additional dimension of validation/cross-check of the GOS approach.

270 In addition, we conducted four sensitivity calculations for Stage I and six sensitivity
271 calculations for Stages II and III to quantify uncertainties associated with BC RI and morphology
272 (see Table 1). In the first sensitivity calculation for each aging stage, a lower bound of BC RI of
273 1.75 - 0.63i recommended by Bond and Bergstrom (2006) was used. For other three sensitivity
274 tests on morphology effects at Stage I, we increased BC fractal dimension from 2.1 to 2.5 and
275 primary spherules diameter from 15 to 20 nm without changing BC mass, and replaced BC
276 aggregates with a single volume-equivalent sphere, respectively. We then applied five types of
277 BC coating structures, including off-center core-shell, closed-cell, open-cell, partially
278 encapsulated, and externally attached structures (see Fig. 1 and Sect. 2.1), and conducted five
279 additional sensitivity calculations for both Stages II and III. Specifically, the off-center core-shell
280 structure assumes a spherical BC core internally tangent to the particle surface with the same size
281 as the concentric core-shell structure used in standard calculations. The closed-cell structure
282 assumes that all primary spherules have the same concentric core-shell shape with a BC core
283 diameter of 15 nm. The open-cell structure also assumes a diameter of 15 nm for all primary
284 spherules, which are either pure BC or pure coating material. Both closed- and open-cell

285 structures were constructed to have the same fractal dimension as measured in the experiments.
286 The partially encapsulated structure assumes that a random part of BC aggregates is inside a
287 spherical coating particle (Figs. S1-S6), while the externally attached structure assumes that a
288 single spherical coating particle is randomly sticking to a part of BC aggregate's surface (Figs.
289 S1-S6). BC primary spherules in both structures have diameters of 15 nm. We note that assuming
290 a cluster of spheres for the above-mentioned coating structures may not be sufficiently realistic
291 and that nonspherical morphology models without restrictions to composite of spheres appear to
292 be more plausible (Adachi et al., 2010), a challenging subject to be investigated in future work.

293

294

295 **2.5 Application to field measurements**

296 ~~We utilized BC measurements from the CalNex aircraft campaign conducted in May 2010~~
297 ~~(<http://www.esrl.noaa.gov/esd/calnex/>) as input to the aging model with GOS approach to~~
298 ~~compute the evolution of BC optical properties and DRF during the transport from the Los~~
299 ~~Angeles (LA) Basin to downwind regions. The BC particle size, coating thickness and fraction,~~
300 ~~coating composition, and vertical profile have been measured during the CalNex campaign~~
301 ~~(Metcalf et al., 2012), which were used to drive theoretical calculations. We used an aggregate~~
302 ~~structure for uncoated BC and a concentric core-shell structure for coated BC. To quantify~~
303 ~~uncertainties associated with BC RI and morphology, we have conducted calculations with BC~~
304 ~~RI of $1.95 - 0.79i$ and $1.75 - 0.63i$ and different particle structures for uncoated/coated BC as~~
305 ~~used in the proceeding comparison with laboratory experiments (see Sect. 2.4). Since the CalNex~~

306 ~~2010 measurements of BC vertical distribution only covers an altitude of 0–3.5 km a.s.l., we have~~
307 ~~used the BC vertical profile within 2.5–10 km a.s.l. observed during the California Air Resources~~
308 ~~Board (CARB) campaign (Koch et al., 2009) as a representative BC vertical distribution in the~~
309 ~~free troposphere over California. The CARB vertical profile was scaled so that the averaged BC~~
310 ~~concentration within 2.5–3.5 km a.s.l. determined from CARB measurements matched CalNex~~
311 ~~measurements.~~

312 ~~The calculated BC optical properties and observed vertical profiles were subsequently used~~
313 ~~as input to the Fu-Liou-Gu (FLG) RTM (Gu et al., 2006, 2010) to compute the instantaneous~~
314 ~~clear-sky BC DRF at the top-of-atmosphere. The FLG RTM combines the delta-four-stream~~
315 ~~approximation for solar flux calculations (Liou et al., 1988) and the delta two/four-stream~~
316 ~~approximation for infrared flux calculations (Fu et al., 1997) to balance accuracy and efficiency.~~
317 ~~The solar (0–5 μm) and infrared (5–50 μm) spectra are divided into 6 and 12 bands, respectively,~~
318 ~~based on the location of absorption band. The correlated k-distribution method (Fu and Liou,~~
319 ~~1992) is used to sort gaseous absorption lines within each band. In this study, we employed the~~
320 ~~monthly mean Goddard Earth Observing System (GEOS-5) meteorological fields for May 2010~~
321 ~~to drive the FLG RTM.~~

322

323 **3. Results and discussions**

324 **3.1 Fresh BC aggregates (Stage I)**

325 Fig. 3 shows the extinction, absorption, and scattering cross sections (at 532 nm) of fresh BC
326 aggregates at Stage I based on laboratory measurements and theoretical calculations using

327 different BC RI and morphology. For comparison with experimental measurements, ~~the averaged~~
328 ~~value for~~ theoretical results ~~with upper and lower bounds of~~ with BC RIs ~~(i.e., of 1.95 – 0.79i and~~
329 ~~1.75 – 0.63i)~~ is (i.e., standard calculations) are used unless stated otherwise. The calculated
330 extinction cross sections are consistent (differences $\leq 20\%$) with measurements for fresh BC
331 aggregates at Stage I with different sizes (i.e., $D_{BC} = 155, 245, \text{ and } 320 \text{ nm}$). However,
332 theoretical calculations tend to overestimate and underestimate extinction for the smallest and
333 largest BC aggregates, respectively. The discrepancies between theoretical and measured BC
334 absorption cross sections at Stage I increase from 37% (overestimate) to 25-15% (underestimate)
335 as BC size becomes larger (Fig. 3). ~~On the contrary, t~~Although the calculated scattering cross
336 sections at Stage I are consistently overestimated for different BC sizes compared with
337 measurements, the absolute discrepancies are small. ~~–~~This overestimate is partly because of the
338 uncertainty associated with extinction and absorption~~theoretical~~ calculations for small particles,
339 where theoretical results overestimate (underestimate) extinction cross sections more (less) than
340 absorption cross sections for D_{BC} of 155 nm (D_{BC} of 245 and 320 nm). The scattering
341 measurements also contribute to the discrepancy in view of the fact that the integrating
342 nephelometer misses light scattering signals at near-forward directions (Anderson and Ogren,
343 1998). We note that the calculated SSA (~ 0.16) of BC aggregates at Stage I is within the range of
344 0.15-0.3 determined—measured for BC from atmospheric observations~~different combustion~~
345 sources (Bond and Bergstrom, 2006), while the experimentally measured SSA is smaller than
346 0.10 due to the relatively open and loosely connected BC aggregate structures (Khalizov et al.,
347 2009a).

348 Sensitivity calculations show that using a BC RI of $1.75 - 0.63i$ narrows the gap between
349 calculated and measured scattering cross sections of fresh BC aggregates by up to a factor of two,
350 ~~while using a BC RI of $1.95 - 0.79i$ reduces underestimates in the calculated BC absorption~~
351 ~~which dominates the extinction at Stage I~~ (Fig. 3). Because of using the BC RIs of $1.95 - 0.79i$
352 (upper bound) and $1.75 - 0.63i$ (lower bound), ~~We found that~~ the extinction, and absorption,
353 ~~and scattering~~ cross sections of fresh BC aggregates can vary by ~~up to 60%~~ 25-40% and 20-30%,
354 respectively, ~~because of applying the BC RI upper or lower bound, in which~~ while the scattering
355 cross section ranges from 50% to 65% with a higher sensitivity for larger BC sizes ~~most~~
356 ~~sensitive~~. Based on the T-matrix calculations using BC RI of $2 - 1i$ and $1.75 - 0.5i$, Liu et al.
357 (2008) showed variation of 50-70% in BC absorption and scattering cross sections depending on
358 aggregate structures, which is comparable to the results derived in this study. Scarnato et al.
359 (2015) also found a strong dependence of BC absorption on BC RI for uncoated aggregates using
360 the DDA method.

361 Fig. 4 shows the extinction, absorption, and scattering cross sections for different aggregate
362 morphology normalized by BC aggregate cross sections determined from standard calculations
363 (i.e., fractal aggregates with a D_f of 2.1 and D_p of 15 nm; see Sect. 2.4) at Stage I. We found that
364 a 20% increase in D_f (i.e., more compact structure) decreases BC absorption and scattering cross
365 sections by 20-50%, with greater reductions for larger BC sizes. Using the DDA method,
366 Scarnato et al. (2013) also found a smaller BC absorption for more compact structures. Liu et al.
367 (2008) applied a T-matrix calculation to show that as D_f increases from 1.5 to 3, the absorption of
368 BC aggregates either decreases monotonically or decreases until D_f reaching a certain value and

369 then increases, depending on BC RI, size and the number of primary spherules. This is because
370 the amount of BC directly exposed to the incident light becomes smaller as D_f increases, while
371 the growing interaction among primary spherules could increase light absorption (Liu et al.,
372 2008). The present calculations illustrated that BC absorption and scattering are weakly
373 dependent on the size of primary BC spherules. An increase in the spherule diameter from 15 to
374 20 nm results in less than 10% variation in BC extinction, absorption, and scattering cross
375 sections (Fig. 4), which is consistent with the T-matrix results presented by Liu and Mishchenko
376 (2007) who concluded that the monomer size has a rather weak effect on BC scattering and
377 absorption, if fractal dimension is fixed. Nevertheless, the effect of monomer size on BC optical
378 properties could vary significantly depending on BC aggregate shape, size, the number of
379 primary spherules, and BC RI (Liu et al., 2008; Kahnert et al., 2014). Assuming a
380 volume-equivalent BC sphere instead of fractal aggregates results in 5-25% weaker absorption
381 and extinction and up to 65% smaller scattering cross sections for different BC sizes, compared
382 with BC aggregates in standard calculations. The stronger absorption and scattering from
383 aggregate structures is due primarily to the interaction between neighboring primary spherules of
384 BC aggregates (Fuller, 1995). The present calculated increase (5-20%) in absorption from sphere
385 to aggregate structures is slightly smaller than the value (~30%) reported by Bond and Bergstrom
386 (2006), because of different numbers and sizes of primary spherules, aggregate shapes, and
387 fractal dimensions employed in calculations (Iskander et al., 1991; Liu et al., 2008; Kahnert et al.,
388 2014). Using the T-matrix method, Kahnert and Devasthale (2011) showed a two times higher
389 radiative forcing of BC aggregates than the volume-equivalent sphere counterparts.

390
391
392
393
394
395
396
397
398
399
400
401
402
403
404
405
406
407
408
409
410

3.2 Coated BC particles (Stages II and III)

The extinction, absorption, and scattering cross sections (at 532 nm) of coated BC particles at aging Stages II and III determined from laboratory measurements and theoretical calculations are depicted in Fig. 3. ~~The theoretical results using with upper and lower bounds of the BC RI of $1.95 - 0.79i$ are averaged-used~~ for comparison with experimental measurements unless stated otherwise. The calculated optical cross sections (i.e., extinction, absorption, and scattering) of coated BC at Stages II and III are in general agreements (differences $\leq 30\%$) with laboratory measurements, because of the observed efficient structure compaction during aging in laboratory experiments (Zhang et al., 2008). However, theoretical calculations tend to overestimate extinction and absorption for D_{BC} of 155 and 245 nm at both Stages II and III, while the extinction and absorption for the largest particle (D_{BC} of 320 nm) is underestimated at Stage II. The calculated scattering cross sections are overestimated for the smallest BC size (D_{BC} of 155 nm) at Stage II, but tend to be underestimated for larger BC sizes at Stage III, particularly for D_{BC} of 320 nm. ~~The calculated cross sections of coated BC at Stages II and III are in good agreement (differences $\leq 20\%$) with laboratory measurements for extinction, absorption, and scattering, except for a 30% underestimate in scattering for D_{BC} of 320 nm at Stage III. This implies that the concentric core-shell model represents the realistic BC coating morphology reasonably well in this case in view of the observed efficient structure compaction during aging (Zhang et al., 2008).~~ The present sensitivity calculations show that the discrepancy in scattering for D_{BC} of 320 nm at Stage III cannot be explained by uncertainties associated with BC RI or

411 coating morphology (Fig. 3), which, however, could be attributed to uncertainty associated with
412 the coating mass of H₂SO₄ and H₂O. We assumed only H₂O condensation during BC
413 hygroscopic growth from Stage II to III in the calculation of coating mass, which may not be
414 accurate considering that H₂SO₄ condenses on BC surface simultaneously along with H₂O. A
415 sensitivity calculation shows that replacing H₂O ~~with~~ by H₂SO₄ in the coating material reduces
416 ~~the scattering discrepancy in scattering~~ to 10% ~~in this case for D_{BC} of 320 nm at Stage III~~, since
417 H₂SO₄ is more reflective than H₂O, ~~but increases overestimate in BC absorption from 17% to~~
418 ~~25%.~~ ~~This also explains the consistent underestimates in the calculated scattering cross sections~~
419 ~~at Stage III for three D_{BC} cases (Fig. 3).~~

420 Theoretical calculations show that using BC RI of ~~1.95 – 0.79i (1.75 – 0.63i)~~ ~~increases~~
421 ~~(decreases)~~ ~~scattering and extinction and~~ absorption cross sections of coated BC particles by
422 10-17% at Stages II_ and by 5-15% at Stage III by up to 30%, for different BC sizes, which,
423 however, is smaller compared with the decrease for fresh BC aggregates (20-40%). ~~where The~~
424 ~~scattering cross sections of coated BC particles decrease by up to 50% due to the use of smaller~~
425 ~~BC RI for different BC sizes and aging stages.~~ ~~is most sensitive to BC RI change. We found that~~
426 ~~the effect of BC RI on extinction and absorption for coated BC particles is similar for different~~
427 ~~BC sizes, but much smaller than the case of fresh BC aggregates.~~

428 Figs. 5 and 6 show the extinction, absorption, and scattering cross sections for different
429 coated BC structures normalized by cross sections of the concentric core-shell structure
430 determined from standard calculations. The off-center core-shell structure has little impacts on
431 BC optical properties at Stage II (Fig. 5) with differences of less than 10% compared with the

432 concentric core-shell structure, primarily because of the thin coating layer. As the coating
433 thickness increases after hygroscopic growth, the off-center core-shell structure results in a 5-30%
434 decrease in extinction, absorption, and scattering cross sections at Stage III (Fig. 6). This finding
435 is consistent with the result presented by Adachi et al. (2010) using the DDA method, where they
436 found up to 30% reductions in BC absorption depending on the position of BC core inside
437 coating material. A recent T-matrix study (Mishchenko et al., 2014) also showed that the
438 absorption of BC-water mixture tends to decrease as a BC particle moves from the droplet center
439 to the boundary.

440 Compared with the concentric core-shell structure, the closed-cell structure tends to have
441 stronger absorption and weaker scattering for D_{BC} of 245 and 320 nm at Stages II and III, while
442 the reverse is true for the open-cell structure (Figs. 5 and 6). This is in line with the conclusion
443 presented in Liou et al. (2011) that closed-cell aggregates have larger absorption and smaller
444 SSA than their open-cell counterparts. The closed-cell structure has a larger surface area for
445 interaction of the incident light with each primary spherule that acts as a coated core-shell unit,
446 leading to a stronger lensing effect and thus stronger absorption compared with the concentric
447 core-shell structure. However, the open-cell structure lacks a closed coating structure to produce
448 efficient lensing effects. The coating spherules sticking to pure BC spherules in the open-cell
449 structure increase the interaction between the incident light and non-absorbing coating material,
450 resulting in a stronger scattering.

451 The extinction and absorption cross sections of partially encapsulated and externally
452 attached structures are consistently lower than those of the concentric core-shell structure by

453 30-80% for different BC sizes (Figs. 5 and 6). This is because the relatively open coating
454 structure leads to inefficient lensing effect for partially encapsulated and externally attached
455 structures, in which a part of BC aggregates is shielded from interaction with incident photons
456 that are backscattered by the attached non-absorbing coating material. Adachi et al. (2010)
457 showed that the concentric core-shell structure has a 20-30% stronger absorption than BC
458 aggregates that are fully embedded within host sulfate. Thus, the partially encapsulated structure
459 with only a part of BC aggregates embedded inside coating material in the present study could
460 further decrease the absorption and lead to much smaller absorption values than a concentric
461 core-shell structure. Kahnert et al. (2013) found that the difference in BC absorption between
462 concentric core-shell and encapsulated structures strongly depends on particle size, BC volume
463 fraction, and wavelength, based on the DDA calculation. Interestingly, we found that the
464 absorption of partially encapsulated structure is 10-40% weaker than that of externally attached
465 structure with larger differences for thicker coating, while their scattering cross sections are
466 similar (differences $\leq 5\%$). The preceding analysis demonstrates that coating structures exert a
467 significant impact on BC optical properties. Thus, in order to produce reliable and accurate
468 estimates of BC radiative forcing in climate models, the development of a realistic BC coating
469 morphology parameterization appears to be essential, which, however, could be a challenging
470 task in view of limited observations available at the present time.-

471

472 **3.3 Evolution of BC absorption and scattering**

473 Fig. 7 shows the enhancement in absorption and scattering during BC aging from freshly

474 emitted aggregates (Stage I) to BC coated by H_2SO_4 (Stage II) and by $H_2SO_4-H_2O$ (Stage III) for
475 different BC coating structures and sizes. The measured BC absorption increases by 10-45% due
476 to coating, while the concentric core-shell model results in a 20-65% absorption increase
477 depending on BC sizes and aging stages. This implies that assuming a concentric core-shell
478 shape could overestimate BC radiative forcing. Adachi et al. (2010) found that using a more
479 realistic BC coating morphology from field measurements leads to about 20% less BC DRF than
480 using a concentric core-shell shape.

481 Moreover, coated BC particles with closed-cell structures enhance absorption by 50-100%
482 for Stage II and more than 100% after hygroscopic growth (Fig. 7). In contrast, the open-cell
483 structures produce less than 10% increase in absorption during aging for D_{BC} of 245 and 320 nm,
484 while the enhancement tends to be stronger for smaller BC size ($D_{BC} = 155$ nm). Surprisingly, we
485 found that the partially encapsulated and externally attached BC structures have a weaker
486 absorption than fresh BC aggregates, probably because that the two structures in the absence of
487 fully embedded shape have no efficient lensing effect and that the non-absorbing coating
488 material blocks the photons coming from behind BC aggregates and produces a shadowing effect
489 (Liu and Mishchenko, 2007). This shadowing effect could also explain the decreasing BC
490 absorption for partially encapsulated, externally attached, and open-cell structures when coating
491 material increases during Stages II to III. Adachi and Buseck (2013) and Scarnato et al. (2013)
492 found that BC particles attached to or partially immersed in host material, instead of fully
493 embedded within them, do not show noticeable increases in BC absorption relative to uncoated
494 aggregates based on DDA calculations. Bond et al. (2006) recommended a 50% increase in BC

495 absorption to account for the averaged coating effect during atmospheric aging. However, in
496 light of the preceding analysis, the morphology, composition and amount of coating play
497 significant roles in altering the BC optical properties during aging. It appears that a fixed
498 enhancement factor may not represent the realistic increase in BC absorption due to complex
499 coating, particularly over regions with highly heterogeneous aging conditions.

500 Compared with absorption enhancement, BC coating results in a much larger increase in
501 scattering, with a greater enhancement for a larger amount of coating material (Fig. 7). The
502 measured scattering cross sections from laboratory experiments for different BC sizes increase
503 by a factor of 5-6 from Stage I to II and a factor of 11-~~12~~-13 from Stage I to III. Theoretical
504 calculations show that ~~tThe calculated~~ increase in scattering from Stage I to II varies from a
505 factor of 3 to 8 for D_{BC} of 245 and 320 nm depending on coating morphology, while both the
506 magnitude and variation of enhancement are much larger for D_{BC} of 155 nm ranging from a
507 factor of 6 to 15. After hygroscopic growth (Stage III), BC scattering further increases by 20-200%
508 for different coating structures relative to that at Stage II. Cheng et al. (2009) observed that the
509 increase in BC scattering, due to both the increased amount of coating and the transition of
510 uncoated to coated BC, can reach up to a factor of 8-10 within several hours' aging at a polluted
511 site in northeastern China, which is comparable to laboratory measurements and theoretical
512 calculations presented above.

513

514 **4. Implication for regional radiative forcing analysis Atmospheric implications**

515 Our theoretical calculations have shown that BC absorption and scattering are highly

516 sensitive to coating morphology and the amount of coating at different aging stages. This
517 suggests that the change of BC coating states (e.g., coating thickness, morphology, and
518 composition) during aging process in the real atmosphere could substantially affect BC radiative
519 properties and thus its climatic effects. Metcalf et al. (2012) observed that the mean BC coating
520 thickness increases from ~95 nm over urban areas within boundary layers to ~150 nm in its
521 downwind regions and ~190 nm in the free troposphere, with a factor of two higher number
522 fractions of thickly coated BC in the free troposphere and downwind regions than near the source.
523 Such large variations in BC coating thickness and number fraction of thickly coated BC during
524 aging have also been observed over the tropics from the ground to high altitudes (Schwarz et al.,
525 2008), implying a strong dependence of BC coating state on aging condition and timescale that
526 BC particles have experienced. Furthermore, atmospheric observations also suggest large
527 variability in the composition of coating materials (Moteki et al. 2007; Metcalf et al., 2012) and
528 coating morphology (China et al., 2013; 2015) during BC aging under different atmospheric
529 conditions. Thus, better characterizations of BC coating mass, composition, and morphology
530 during aging are critically important to accurately estimate BC radiative effects.

531 However, many global models tend to use fixed BC optical properties or simplified
532 core-shell models for the computation of BC radiative effects (Bond et al., 2013), which may not
533 be representative and sufficiently accurate in view of various BC coating states in the real
534 atmosphere. This study suggests that a reliable estimate of BC radiative effects in climate models
535 would require the representation of a dynamic BC aging process with realistic coating structures,
536 especially for regional analysis with highly heterogeneous atmospheric conditions.

537 Fig. 8 presents the evolution of BC coating fraction and thickness, optical properties, and
538 DRF during the transport from the source region (LA Basin) to ~200 km downwind regions
539 during the CalNex 2010 campaign, including West and East LA Basin, Banning Pass, Banning
540 Outflow, and Imperial Valley. The observed BC loads decrease by a factor of three during
541 transport (Fig. 8c) as a result of the dilution by cleaner air, while the observed BC coating
542 thickness and fraction increase by a factor of two (Figs. 8a, b) revealing a strong BC aging
543 during transport (Metcalf et al., 2012). The present calculations show that the effective BC MAC
544 (i.e., the sum of coated and uncoated BC MAC weighted by their mass fractions) and SSA
545 increases from 10 to 13 m² g⁻¹ (Fig. 8d) and 0.4 to 0.6 (Fig. 8e), respectively, due to coating
546 during aging. The BC DRF increases from 1.5 to 1.7 W m⁻² from West to East LA Basin and
547 decreases rapidly to ~1.0 W m⁻² from East LA Basin to Imperial Valley (Fig. 8f), which is
548 associated with the absorption enhancement produced by coating that dominates the
549 DRF increasing period and BC concentration dilution that dominates the DRF decreasing period.
550 The BC DRF over the LA Basin and downwind regions in this case is more than a factor of two
551 higher than the annual mean value over California (Wang et al., 2014) and a factor of 1.5–2
552 higher than the global annual mean value (Bond et al., 2013). The present analysis shows that the
553 BC DRF varies by 20% due to the use of upper and lower bounds of BC RI and by a factor of
554 two depending on different BC morphology (Fig. 8f). Thus, it is important to incorporate a
555 realistic representation of BC structure and its parameterization in climate models in order to
556 accurately capture regional BC DRF evolution.

557 In this conjunction, many global atmospheric models tend to use a fixed BC MAC for DRF

558 ~~estimates in the absence of BC aging microphysics (e.g., Schulz et al., 2006; Wang et al., 2014).~~
559 ~~We found that using a fixed BC MAC of $11.3 \text{ m}^2 \text{ g}^{-1}$ that represents the mean BC mixing state~~
560 ~~from atmospheric observations (Bond et al., 2006), the BC DRF decreases monotonically from~~
561 ~~2.1 to 0.8 W m^{-2} from the LA Basin to downwind regions, with up to 40% differences in~~
562 ~~individual subregions, as compared with the DRF determined from the evolved BC MAC~~
563 ~~accounting for the change of BC optical properties during aging. Consequently, a fixed BC MAC~~
564 ~~for the mean mixing state may not be representative and sufficiently accurate within the context~~
565 ~~of regional radiative forcing analysis, which would require the use of a dynamic BC aging~~
566 ~~process coupled with the evolution of radiative properties in climate models.~~

567

568 **5. Conclusions**

569 We developed a theoretical model that accounts for three typical BC aging stages, including
570 freshly emitted aggregates, coated BC by soluble material, and coated BC particles after further
571 hygroscopic growth. The GOS approach was used to compute BC absorption and scattering at
572 each aging stage, which was coupled with a stochastic procedure to construct different BC
573 structures. The theoretical calculations were compared with laboratory measurements, followed
574 by a systematic analysis on uncertainties associated with BC RI and morphology. Finally, we
575 discussed atmospheric implications of our results in the assessment of BC radiative
576 effects.~~applied the theoretical aging model and GOS approach to investigate the evolution of BC~~
577 ~~radiative properties and DRF during the transport from the LA Basin to downwind regions, based~~
578 ~~on the CalNex 2010 field measurements.~~

579 Theoretical calculations yielded consistent extinction (sum of absorption and scattering)
580 cross sections for fresh BC aggregates at Stage I, with differences of less than 20% compared
581 with measurements. Theoretical calculations underestimated BC absorption by up to 25%, while
582 overestimated BC scattering for different sizes, because of uncertainties ~~involved~~ associated with
583 both theoretical calculations for small particles and scattering measurements in laboratory
584 experiments. Sensitivity calculations showed that variation of ~~optical~~ the extinction and
585 absorption cross sections of fresh BC aggregates ~~can be~~ is up to 60% ~~20-40%~~ due to the use of
586 ~~different upper and lower bounds of BC RIs, in which~~ while the variation of the scattering cross
587 section is most sensitive ranges from 50% to 65% with a higher sensitivity for larger BC sizes.
588 We also found that the optical cross sections of BC aggregates are sensitive to D_f , but insensitive
589 to the size of primary spherules. Using volume-equivalent spheres instead of aggregates
590 decreased the BC absorption at Stage I.

591 The measured extinction, absorption, and scattering cross sections of coated BC were
592 generally captured (differences \leq ~~20~~ 30%) by theoretical calculations using a concentric
593 core-shell structure for Stages II and III. However, theoretical calculations tend to overestimate
594 extinction and absorption for D_{BC} of 155 and 245 nm at Stages II and III, while the scattering
595 tends to be underestimated for larger BC sizes at Stage III, particularly for D_{BC} of 320 nm due
596 partly to the uncertainty associated with H_2SO_4 - H_2O coating mass. ~~although the scattering at~~
597 ~~Stage III for D_{BC} of 320 nm was underestimated by about 30% because of uncertainties~~
598 ~~associated with H_2SO_4 - H_2O coating mass.~~ Sensitivity analyses showed that the effects of BC RI
599 on extinction and absorption for coated BC were much smaller than that for fresh BC aggregates.

600 The off-center core-shell structure resulted in up to 30% less absorption and scattering cross
601 sections than the concentric core-shell structure. The open-cell structure tended to have weaker
602 absorption and stronger scattering than the concentric core-shell structure, while the reverse is
603 true for the closed-cell structure. Compared with the concentric core-shell structure, the partially
604 encapsulated and externally attached structures had substantially smaller absorption and
605 scattering cross sections due to the lack of efficient lensing effects.

606 Theoretical calculations showed that using a concentric core-shell structure slightly
607 overestimated the measured enhancement in BC absorption by up to 30% during aging. The
608 closed-cell structure led to a factor of two higher increases in BC absorption than measured
609 values, while the open-cell structure did not show a noticeable increase in absorption for D_{BC} of
610 245 and 320 nm during aging. The partially encapsulated and externally attached coating
611 structures had a weaker absorption than fresh BC aggregates, likely produced by the shadowing
612 effect from non-absorbing coating material as well as the lack of efficient lensing effect. The
613 increase in BC scattering during aging was much stronger than absorption, ranging from a factor
614 of 3 to 24 depending on BC size, morphology, and aging stage. Thus, the present analysis
615 suggested ~~showed~~ that BC optical properties are highly sensitive to BC morphology and ~~the~~
616 ~~amount and composition of coating~~ coating mass at different aging stages ~~exert significant impacts~~
617 ~~on the BC optical properties. Therefore, it is critically important to incorporate realistic BC~~
618 ~~coating properties in climate models for an accurate estimate of BC radiative forcing.~~

619 Our theoretical calculations suggested that the evolution of BC coating states (e.g., coating
620 thickness, morphology, and composition) during aging in the real atmosphere could exert

621 significant impacts on BC radiative properties and thus its climatic effects, particularly over
622 regions with high heterogeneity. Therefore, to accurately estimate BC radiative effects requires
623 the incorporation of a dynamic BC aging process accounting for realistic coating structures in
624 climate models.

625 ~~The CalNex field measurements showed a strong BC aging during its transport from the LA~~
626 ~~Basin to downwind regions. The resulting BC DRF first increased from 1.5 to 1.7 W m⁻² and~~
627 ~~subsequently decreased to 1.0 W m⁻², as a result of the competition between BC absorption~~
628 ~~increase due to coating and BC concentration dilution. The present results revealed that BC DRF~~
629 ~~estimate is highly sensitive to BC morphology during aging. Thus, a reliable estimate of BC~~
630 ~~radiative forcing in climate models would require the representation of a dynamic BC aging~~
631 ~~process, including realistic coating structures, especially for regional analysis under highly~~
632 ~~heterogeneous atmospheric conditions.~~

633

634 **Acknowledgement**

635 This research was supported by the NSF under Grant AGS-0946315 and AGS-1523296, by
636 the DOE Earth System Modeling program under Grant DESC0006742, and by Subcontract
637 S100097 from the Texas A&M Research Foundation, which is sponsored by NASA under Grant
638 NNX11AK39G. Pacific Northwest National Laboratory is operated for DOE by Battelle
639 Memorial Institute under contract DE-AC05-76RL01830. R. Zhang acknowledges the support by
640 the Robert A. Welch Foundation (A-1417). The authors thank all the contributors to the CalNex
641 and CARB field measurements. Users can access the data in this study through the corresponding
642 author.

643

644 **References**

- 645 Adachi, K., and Buseck, P. R.: Changes of ns-soot mixing states and shapes in an urban area
646 during CalNex, *J. Geophys. Res.-Atmos.*, 118, 3723-3730, doi:10.1002/Jgrd.50321, 2013.
- 647 Adachi, K., Chung, S. H., and Buseck, P. R.: Shapes of soot aerosol particles and implications
648 for their effects on climate, *J. Geophys. Res.-Atmos.*, 115, D15206,
649 doi:10.1029/2009jd012868, 2010.
- 650 Anderson, T. L., and Ogren, J. A.: Determining aerosol radiative properties using the TSI 3563
651 integrating nephelometer, *Aerosol Sci. Tech.*, 29, 57-69, doi:10.1080/02786829808965551,
652 1998.
- 653 Bond, T. C., and Bergstrom, R. W.: Light absorption by carbonaceous particles: An investigative
654 review, *Aerosol Sci. Tech.*, 40, 27-67, doi:10.1080/02786820500421521, 2006.
- 655 Bond, T. C., Habib, G., and Bergstrom, R. W.: Limitations in the enhancement of visible light
656 absorption due to mixing state, *J. Geophys. Res.-Atmos.*, 111, D20211,
657 doi:10.1029/2006jd007315, 2006.
- 658 Bond, T. C., Doherty, S. J., Fahey, D. W., Forster, P. M., Berntsen, T., DeAngelo, B. J., Flanner,
659 M. G., Ghan, S., Karcher, B., Koch, D., Kinne, S., Kondo, Y., Quinn, P. K., Sarofim, M. C.,
660 Schultz, M. G., Schulz, M., Venkataraman, C., Zhang, H., Zhang, S., Bellouin, N.,
661 Guttikunda, S. K., Hopke, P. K., Jacobson, M. Z., Kaiser, J. W., Klimont, Z., Lohmann, U.,
662 Schwarz, J. P., Shindell, D., Storelvmo, T., Warren, S. G., and Zender, C. S.: Bounding the
663 role of black carbon in the climate system: A scientific assessment, *J. Geophys. Res.-Atmos.*,
664 118, 5380-5552, doi:10.1002/Jgrd.50171, 2013.
- 665 [Born, M., and Wolf, E.: Principles of Optics: electromagnetic theory of propagation, interference](#)
666 [and diffraction of light, 7th ed., Cambridge University Press, UK, 636-637, 1999.](#)
- 667 Cheng, Y. F., Berghof, M., Garland, R. M., Wiedensohler, A., Wehner, B., Muller, T., Su, H.,
668 Zhang, Y. H., Achtert, P., Nowak, A., Poschl, U., Zhu, T., Hu, M., and Zeng, L. M.:
669 Influence of soot mixing state on aerosol light absorption and single scattering albedo
670 during air mass aging at a polluted regional site in northeastern China, *J. Geophys.*
671 *Res.-Atmos.*, 114, D00g10, doi:10.1029/2008jd010883, 2009.
- 672 China, S., Mazzoleni, C., Gorkowski, K., Aiken, A. C., and Dubey, M. K.: Morphology and
673 mixing state of individual freshly emitted wildfire carbonaceous particles, *Nat. Commun.*, 4,
674 2122, doi:10.1038/ncomms3122, 2013.
- 675 China, S., Scarnato, B., Owen, R. C., Zhang, B., Ampadu, M. T., Kumar, S., Dzepina, K.,
676 Dziobak, M. P., Fialho, P., Perlinger, J. A., Hueber, J., Helmig, D., Mazzoleni, L. R., and
677 Mazzoleni, C.: Morphology and mixing state of aged soot particles at a remote marine free
678 troposphere site: Implications for optical properties, *Geophys. Res. Lett.*, 42, 1243-1250,
679 doi:10.1002/2014gl062404, 2015.
- 680 Cappa, C. D., Onasch, T. B., Massoli, P., Worsnop, D. R., Bates, T. S., Cross, E. S., Davidovits,
681 P., Hakala, J., Hayden, K. L., Jobson, B. T., Kolesar, K. R., Lack, D. A., Lerner, B. M., Li, S.
682 M., Mellon, D., Nuaaman, I., Olfert, J. S., Petaja, T., Quinn, P. K., Song, C., Subramanian,
683 R., Williams, E. J., and Zaveri, R. A.: Radiative Absorption Enhancements Due to the

684 Mixing State of Atmospheric Black Carbon, *Science*, 337, 1078-1081,
685 doi:10.1126/science.1223447, 2012.

686 Decesari, S., Facchini, M. C., Matta, E., Mircea, M., Fuzzi, S., Chughtai, A. R., and Smith, D. M.:
687 Water soluble organic compounds formed by oxidation of soot, *Atmos. Environ.*, 36,
688 1827-1832, doi:10.1016/S1352-2310(02)00141-3, 2002.

689 Draine, B. T., and Flatau, P. J.: Discrete-Dipole Approximation for Scattering Calculations, *J.*
690 *Opt. Soc. Am. A*, 11, 1491-1499, doi:10.1364/Josaa.11.001491, 1994.

691 ~~Fu, Q., and Liou, K. N.: On the Correlated K Distribution Method for Radiative Transfer in~~
692 ~~Nonhomogeneous Atmospheres, *J. Atmos. Sci.*, 49, 2139-2156,~~
693 ~~doi:10.1175/1520-0469(1992)049<2139:Otedmf>2.0.Co;2, 1992.~~

694 ~~Fu, Q., Liou, K. N., Cribb, M. C., Charlock, T. P., and Grossman, A.: Multiple scattering~~
695 ~~parameterization in thermal infrared radiative transfer, *J. Atmos. Sci.*, 54, 2799-2812,~~
696 ~~doi:10.1175/1520-0469(1997)054<2799:Mspiti>2.0.Co;2, 1997.~~

697 Fuller, K. A.: Scattering and Absorption Cross-Sections of Compounded Spheres .2. Calculations
698 for External Aggregation, *J. Opt. Soc. Am. A*, 12, 881-892, doi:10.1364/Josaa.12.000881,
699 1995.

700 Gangl, M., Kocifaj, M., Videen, G., and Horvath, H.: Light absorption by coated nano-sized
701 carbonaceous particles, *Atmos. Environ.*, 42, 2571-2581,
702 doi:10.1016/j.atmosenv.2007.05.030, 2008.

703 ~~Gu, Y., Liou, K. N., Xue, Y., Mechoso, C. R., Li, W., and Luo, Y.: Climatic effects of different~~
704 ~~aerosol types in China simulated by the UCLA general circulation model, *J. Geophys.*~~
705 ~~*Res. Atmos.*, 111, D15201, doi:10.1029/2005jd006312, 2006.~~

706 ~~Gu, Y., Liou, K. N., Chen, W., and Liao, H.: Direct climate effect of black carbon in China and~~
707 ~~its impact on dust storms, *J. Geophys. Res. Atmos.*, 115, D00k14,~~
708 ~~doi:10.1029/2009jd013427, 2010.~~

709 He, C., Li, Q. B., Liou, K. N., Takano, Y., Gu, Y., Qi, L., Mao, Y. H., and Leung, L. R.: Black
710 carbon radiative forcing over the Tibetan Plateau, *Geophys. Res. Lett.*, 41, 7806-7813,
711 doi:10.1002/2014gl062191, 2014.

712 Heintzenberg, J., and Covert, D. S.: Size Distribution of Elemental Carbon, Sulfur and Total Mass
713 in the Radius Range 10^{-6} to 10^{-4} cm, *Sci. Total Environ.*, 36, 289-297,
714 doi:10.1016/0048-9697(84)90279-1, 1984.

715 Heintzenberg, J.: Fine particles in the global troposphere: A review, *Tellus B*, 41, 149-160,
716 doi:10.1111/j.1600-0889.1989.tb00132.x, 1989.

717 Iskander, M. F., Chen, H. Y., and Penner, J. E.: Resonance Optical-Absorption by Fractal
718 Agglomerates of Smoke Aerosols, *Atmos. Environ.*, 25, 2563-2569,
719 doi:10.1016/0960-1686(91)90173-5, 1991.

720 Jacobson, M. Z.: Strong radiative heating due to the mixing state of black carbon in atmospheric
721 aerosols. *Nature*, 409, 695-697, doi:10.1038/35055518, 2001.

722 Jacobson, M. Z.: Effects of biomass burning on climate, accounting for heat and moisture fluxes,
723 black and brown carbon, and cloud absorption effects, *J. Geophys. Res. Atmos.*, 119,
724 8980-9002, doi:10.1002/2014JD021861, 2014.

725 Johnson, K. S., Zuberi, B., Molina, L. T., Molina, M. J., Iedema, M. J., Cowin, J. P., Gaspar, D. J.,
726 Wang, C., and Laskin, A.: Processing of soot in an urban environment: case study from the
727 Mexico City Metropolitan Area, *Atmos. Chem. Phys.*, 5, 3033-3043, 2005.

728 Kahnert, M., and Devasthale, A.: Black carbon fractal morphology and short-wave radiative
729 impact: a modelling study, *Atmos. Chem. Phys.*, 11, 11745-11759,
730 doi:10.5194/acp-11-11745-2011, 2011.

731 Kahnert, M., Nousiainen, T., and Lindqvist, H.: Models for integrated and differential scattering
732 optical properties of encapsulated light absorbing carbon aggregates, *Opt. Express.*, 21,
733 7974-7993, doi:10.1364/Oe.21.007974, 2013.

734 Kahnert, M., Nousiainen, T., and Lindqvist, H.: Review: Model particles in atmospheric optics, *J.*
735 *Quant. Spectrosc. Radiat. Transfer*, 146, 41-58, doi:10.1016/j.jqsrt.2014.02.014, 2014.

736 Kasper, M., Siegmann, K., and Sattler, K.: Evaluation of an in situ sampling probe for its
737 accuracy in determining particle size distributions from flames, *J. Aerosol Sci.*, 28,
738 1569-1578, doi:10.1016/S0021-8502(97)00031-1, 1997.

739 Khalizov, A. F., Xue, H. X., Wang, L., Zheng, J., and Zhang, R. Y.: Enhanced Light Absorption
740 and Scattering by Carbon Soot Aerosol Internally Mixed with Sulfuric Acid, *J. Phys. Chem.*
741 *A*, 113, 1066-1074, doi:10.1021/Jp807531n, 2009.

742 Khalizov, A. F., Zhang, R. Y., Zhang, D., Xue, H. X., Pagels, J., and McMurry, P. H.: Formation
743 of highly hygroscopic soot aerosols upon internal mixing with sulfuric acid vapor, *J.*
744 *Geophys. Res.-Atmos.*, 114, D05208, doi:10.1029/2008jd010595, 2009.

745 Khalizov, A. F., Cruz-Quinones, M., and Zhang, R. Y.: Heterogeneous Reaction of NO₂ on
746 Fresh and Coated Soot Surfaces, *J. Phys. Chem. A*, 114, 7516-7524, doi:10.1021/Jp1021938,
747 2010.

748 Knox, A., Evans, G. J., Brook, J. R., Yao, X., Jeong, C. H., Godri, K. J., Sabaliauskas, K., and
749 Slowik, J. G.: Mass Absorption Cross-Section of Ambient Black Carbon Aerosol in
750 Relation to Chemical Age, *Aerosol Sci. Tech.*, 43, 522-532,
751 doi:10.1080/02786820902777207, 2009.

752 ~~Koch, D., Schulz, M., Kinne, S., McNaughton, C., Spaakman, J. R., Balkanski, Y., Bauer, S.,~~
753 ~~Berntsen, T., Bond, T. C., Boucher, O., Chin, M., Clarke, A., De Luca, N., Dentener, F.,~~
754 ~~Diehl, T., Dubovik, O., Easter, R., Fahey, D. W., Feichter, J., Fillmore, D., Freitag, S., Ghan,~~
755 ~~S., Ginoux, P., Gong, S., Horowitz, L., Iversen, T., Kirkevag, A., Klimont, Z., Kondo, Y.,~~
756 ~~Krol, M., Liu, X., Miller, R., Montanaro, V., Moteki, N., Myhre, G., Penner, J. E., Perlwitz,~~
757 ~~J., Pitari, G., Reddy, S., Sahu, L., Sakamoto, H., Schuster, G., Schwarz, J. P., Seland, O.,~~
758 ~~Stier, P., Takegawa, N., Takemura, T., Textor, C., van Aardenne, J. A., and Zhao, Y.:~~
759 ~~Evaluation of black carbon estimations in global aerosol models, *Atmos. Chem. Phys.*, 9,~~
760 ~~9001-9026, 2009.~~

761 Kondo, Y., Matsui, H., Moteki, N., Sahu, L., Takegawa, N., Kajino, M., Zhao, Y., Cubison, M. J.,
762 Jimenez, J. L., Vay, S., Diskin, G. S., Anderson, B., Wisthaler, A., Mikoviny, T., Fuelberg,
763 H. E., Blake, D. R., Huey, G., Weinheimer, A. J., Knapp, D. J., and Brune, W. H.:
764 Emissions of black carbon, organic, and inorganic aerosols from biomass burning in North
765 America and Asia in 2008, *J. Geophys. Res.-Atmos.*, 116, D08204,

766 doi:10.1029/2010jd015152, 2011.

767 Lack, D. A., Langridge, J. M., Bahreini, R., Cappa, C. D., Middlebrook, A. M., and Schwarz, J.
768 P.: Brown carbon and internal mixing in biomass burning particles, *P. Natl. Acad. Sci. USA*,
769 109, 14802-14807, doi:10.1073/pnas.1206575109, 2012.

770 ~~Liou, K. N., Fu, Q., and Ackerman, T. P.: A Simple Formulation of the Delta-4 Stream~~
771 ~~Approximation for Radiative Transfer Parameterizations, *J. Atmos. Sci.*, 45, 1940-1947,~~
772 ~~doi:10.1175/1520-0469(1988)045<1940:Asfotd>2.0.Co;2, 1988.~~

773 Liou, K. N., Takano, Y., and Yang, P.: On geometric optics and surface waves for light
774 scattering by spheres, *J. Quant. Spectrosc. Radiat. Transfer*, 111, 1980-1989,
775 doi:10.1016/j.jqsrt.2010.04.004, 2010.

776 Liou, K. N., Takano, Y., and Yang, P.: Light absorption and scattering by aggregates:
777 Application to black carbon and snow grains, *J. Quant. Spectrosc. Radiat. Transfer*, 112,
778 1581-1594, doi:10.1016/j.jqsrt.2011.03.007, 2011.

779 Liou, K. N., Takano, Y., He, C., Yang, P., Leung, L. R., Gu, Y., and Lee, W. L.: Stochastic
780 parameterization for light absorption by internally mixed BC/dust in snow grains for
781 application to climate models, *J. Geophys. Res.-Atmos.*, 119, 7616-7632,
782 doi:10.1002/2014jd021665, 2014.

783 Liu, L., and Mishchenko, M. I.: Scattering and radiative properties of complex soot and
784 soot-containing aggregate particles, *J. Quant. Spectrosc. Radiat. Transfer*, 106, 262-273,
785 doi:10.1016/j.jqsrt.2007.01.020, 2007.

786 Liu, L., Mishchenko, M. I., and Arnott, W. P.: A study of radiative properties of fractal soot
787 aggregates using the superposition T-matrix method, *J. Quant. Spectrosc. Radiat. Transfer*,
788 109, 2656-2663, doi:10.1016/j.jqsrt.2008.05.001, 2008.

789 Mackowski, D. W., and Mishchenko, M. I.: Calculation of the T matrix and the scattering matrix
790 for ensembles of spheres, *J. Opt. Soc. Am. A*, 13, 2266-2278, doi:10.1364/Josaa.13.002266,
791 1996.

792 Martins, J. V., Artaxo, P., Liousse, C., Reid, J. S., Hobbs, P. V., and Kaufman, Y. J.: Effects of black
793 carbon content, particle size, and mixing on light absorption by aerosols from biomass
794 burning in Brazil, *J. Geophys. Res.-Atmos.*, 103, 32041-32050, doi:10.1029/98jd02593,
795 1998.

796 Metcalf, A. R., Craven, J. S., Ensberg, J. J., Brioude, J., Angevine, W., Sorooshian, A., Duong, H.
797 T., Jonsson, H. H., Flagan, R. C., and Seinfeld, J. H.: Black carbon aerosol over the Los
798 Angeles Basin during CalNex, *J. Geophys. Res.-Atmos.*, 117, D00v13,
799 doi:10.1029/2011jd017255, 2012.

800 Mishchenko, M. I., Liu, L., Cairns, B., and Mackowski, D. W.: Optics of water cloud droplets
801 mixed with black-carbon aerosols, *Opt. Lett.*, 39, 2607-2610, doi:10.1364/Ol.39.002607,
802 2014.

803 ~~Moffet, R. C., and Prather, K. A.: In situ measurements of the mixing state and optical properties~~
804 ~~of soot with implications for radiative forcing estimates, *P. Natl. Acad. Sci. USA*, 106,~~
805 ~~11872-11877, doi:10.1073/pnas.0900040106, 2009.~~

806 Moteki, N., Kondo, Y., Miyazaki, Y., Takegawa, N., Komazaki, Y., Kurata, G., Shirai, T., Blake,

807 D. R., Miyakawa, T., and Koike, M.: Evolution of mixing state of black carbon particles:
808 Aircraft measurements over the western Pacific in March 2004, *Geophys. Res. Lett.*, 34,
809 L11803, doi:10.1029/2006gl028943, 2007.

810 ~~Naoe, H., Hasegawa, S., Heintzenberg, J., Okada, K., Uchiyama, A., Zaizen, Y., Kobayashi, E.,
811 and Yamazaki, A.: State of mixture of atmospheric submicrometer black carbon particles
812 and its effect on particulate light absorption, *Atmos. Environ.*, 43, 1296-1301,
813 doi:10.1016/j.atmosenv.2008.11.031, 2009.~~

814 Nussenzveig, H. M., and Wiscombe, W. J.: Efficiency Factors in Mie Scattering, *Phys. Rev.*
815 *Lett.*, 45, 1490-1494, doi:10.1103/PhysRevLett.45.1490, 1980.

816 Pagels, J., Khalizov, A. F., McMurry, P. H., and Zhang, R. Y.: Processing of Soot by Controlled
817 Sulphuric Acid and Water Condensation Mass and Mobility Relationship, *Aerosol Sci. Tech.*,
818 43, 629-640, doi:10.1080/02786820902810685, 2009.

819 Popovicheva, O. B., Persiantseva, N. M., Kireeva, E. D., Khokhlova, T. D., and Shonija, N. K.:
820 Quantification of the Hygroscopic Effect of Soot Aging in the Atmosphere: Laboratory
821 Simulations, *J. Phys. Chem. A*, 115, 298-306, doi:10.1021/Jp109238x, 2011.

822 Qiu, C., Khalizov, A. F., and Zhang, R. Y.: Soot Aging from OH-Initiated Oxidation of Toluene,
823 *Environ. Sci. Technol.*, 46, 9464-9472, doi:10.1021/Es301883y, 2012.

824 Ramanathan, V., and Carmichael, G.: Global and regional climate changes due to black carbon,
825 *Nat. Geosci.*, 1, 221-227, doi:10.1038/Ngeo156, 2008.

826 Saathoff, H., Naumann, K. H., Schnaiter, M., Schock, W., Mohler, O., Schurath, U., Weingartner,
827 E., Gysel, M., and Baltensperger, U.: Coating of soot and (NH₄)₂SO₄ particles by ozonolysis
828 products of alpha-pinene, *J. Aerosol Sci.*, 34, 1297-1321,
829 doi:10.1016/S0021-8502(03)00364-1, 2003.

830 Santoro, R. J., Semerjian, H. G., and Dobbins, R. A.: Soot Particle Measurements in Diffusion
831 Flames, *Combust. Flame*, 51, 203-218, doi:10.1016/0010-2180(83)90099-8, 1983.

832 Sedlacek, A. J., Lewis, E. R., Kleinman, L., Xu, J. Z., and Zhang, Q.: Determination of and
833 evidence for non-core-shell structure of particles containing black carbon using the
834 Single-Particle Soot Photometer (SP2), *Geophys. Res. Lett.*, 39, L06802,
835 doi:10.1029/2012gl050905, 2012.

836 Scarnato, B. V., Vahidinia, S., Richard, D. T., and Kirchstetter, T. W.: Effects of internal mixing
837 and aggregate morphology on optical properties of black carbon using a discrete dipole
838 approximation model, *Atmos. Chem. Phys.*, 13, 5089-5101, doi:10.5194/acp-13-5089-2013,
839 2013.

840 Scarnato, B. V., China, S., Nielsen, K., and Mazzoleni, C.: Perturbations of the optical properties
841 of mineral dust particles by mixing with black carbon: a numerical simulation study, *Atmos.*
842 *Chem. Phys.*, 15, 6913-6928, doi:10.5194/acp-15-6913-2015, 2015.

843 ~~Schnaiter, M., Horvath, H., Mohler, O., Naumann, K. H., Saathoff, H., and Schock, O. W.:
844 UV-VIS-NIR spectral optical properties of soot and soot-containing aerosols, *J. Aerosol Sci.*,
845 34, 1421-1444, doi:10.1016/S0021-8502(03)00361-6, 2003.~~

846 ~~Schulz, M., Textor, C., Kinne, S., Balkanski, Y., Bauer, S., Berntsen, T., Berglen, T., Boucher,
847 O., Dentener, F., Guibert, S., Isaksen, I. S. A., Iversen, T., Koch, D., Kirkevag, A., Liu, X.,~~

848 ~~Montanaro, V., Myhre, G., Penner, J. E., Pitari, G., Reddy, S., Seland, O., Stier, P., and~~
849 ~~Takemura, T.: Radiative forcing by aerosols as derived from the AeroCom present-day and~~
850 ~~pre-industrial simulations, *Atmos. Chem. Phys.*, 6, 5225-5246, 2006.~~

851 Schwarz, J. P., Spackman, J. R., Fahey, D. W., Gao, R. S., Lohmann, U., Stier, P., Watts, L. A.,
852 Thomson, D. S., Lack, D. A., Pfister, L., Mahoney, M. J., Baumgardner, D., Wilson, J. C.,
853 and Reeves, J. M.: Coatings and their enhancement of black carbon light absorption in the
854 tropical atmosphere, *J. Geophys. Res.-Atmos.*, 113, D03203, doi:10.1029/2007jd009042,
855 2008.

856 Shiraiwa, M., Kondo, Y., Moteki, N., Takegawa, N., Miyazaki, Y., and Blake, D. R.: Evolution
857 of mixing state of black carbon in polluted air from Tokyo, *Geophys. Res. Lett.*, 34, L16803,
858 doi:10.1029/2007gl029819, 2007.

859 Shiraiwa, M., Kondo, Y., Iwamoto, T., and Kita, K.: Amplification of Light Absorption of Black
860 Carbon by Organic Coating, *Aerosol Sci. Tech.*, 44, 46-54,
861 doi:10.1080/02786820903357686, 2010.

862 Stratmann, F., Bilde, M., Dusek, U., Frank, G. P., Hennig, T., Henning, S., Kiendler-Scharr, A.,
863 Kiselev, A., Kristensson, A., Lieberwirth, I., Mentel, T. F., Poschl, U., Rose, D., Schneider,
864 J., Snider, J. R., Tillmann, R., Walter, S., and Wex, H.: Examination of laboratory-generated
865 coated soot particles: An overview of the LACIS Experiment in November (LExNo)
866 campaign, *J. Geophys. Res.-Atmos.*, 115, D11203, doi:10.1029/2009jd012628, 2010.

867 Strawa, A. W., Drdla, K., Ferry, G. V., Verma, S., Poeschel, R. F., Yasuda, M., Salawitch, R. J.,
868 Gao, R. S., Howard, S. D., Bui, P. T., Loewenstein, M., Elkins, J. W., Perkins, K. K., and
869 Cohen, R.: Carbonaceous aerosol (Soot) measured in the lower stratosphere during
870 POLARIS and its role in stratospheric photochemistry, *J. Geophys. Res.-Atmos.*, 104,
871 26753-26766, doi:10.1029/1999jd900453, 1999.

872 Takano, Y., Liou, K. N., Kahnert, M., and Yang, P.: The single-scattering properties of black
873 carbon aggregates determined from the geometric-optics surface-wave approach and the
874 T-matrix method, *J. Quant. Spectrosc. Radiat. Transfer*, 125, 51-56,
875 doi:10.1016/j.jqsrt.2013.04.006, 2013.

876 Toon, O. B., and Ackerman, T. P.: Algorithms for the Calculation of Scattering by Stratified
877 Spheres, *Appl. Optics.*, 20, 3657-3660, doi:10.1364/Ao.20.003657, 1981.

878 Videen, G., Ngo, D., and Chylek, P.: Effective-Medium Predictions of Absorption by Graphitic
879 Carbon in Water Droplets, *Opt. Lett.*, 19, 1675-1677, doi:10.1364/Ol.19.001675, 1994.

880 ~~Wang, Q. Q., Jacob, D. J., Spackman, J. R., Perring, A. E., Schwarz, J. P., Moteki, N., Marais, E.~~
881 ~~A., Ge, C., Wang, J., and Barrett, S. R. H.: Global budget and radiative forcing of black~~
882 ~~carbon aerosol: Constraints from pole-to-pole (HIPPO) observations across the Pacific, *J.*~~
883 ~~*Geophys. Res.-Atmos.*, 119, 195-206, doi:10.1002/2013jd020824, 2014.~~

884 Wang, Y., Khalizov, A., Levy, M., and Zhang, R. Y.: New Directions: Light absorbing aerosols
885 and their atmospheric impacts, *Atmos. Environ.*, 81, 713-715,
886 doi:10.1016/j.atmosenv.2013.09.034, 2013.

887 Weingartner, E., Burtscher, H., and Baltensperger, U.: Hygroscopic properties of carbon and diesel
888 soot particles, *Atmos. Environ.*, 31, 2311-2327, doi:10.1016/S1352-2310(97)00023-X, 1997.

889 Xue, H. X., Khalizov, A. F., Wang, L., Zheng, J., and Zhang, R. Y.: Effects of dicarboxylic acid
890 coating on the optical properties of soot, *Phys. Chem. Chem. Phys.*, 11, 7869-7875,
891 doi:10.1039/B904129j, 2009.

892 Yang, P., and Liou, K. N.: Finite-difference time domain method for light scattering by small ice
893 crystals in three-dimensional space, *J. Opt. Soc. Am. A*, 13, 2072-2085,
894 doi:10.1364/Josaa.13.002072, 1996.

895 Yang, P., and Liou, K. N.: Light scattering by hexagonal ice crystals: solutions by a ray-by-ray
896 integration algorithm, *J. Opt. Soc. Am. A*, 14, 2278-2289, doi:10.1364/Josaa.14.002278,
897 1997.

898 Zhang, R. Y., Khalizov, A. F., Pagels, J., Zhang, D., Xue, H. X., and McMurry, P. H.: Variability
899 in morphology, hygroscopicity, and optical properties of soot aerosols during atmospheric
900 processing, *P. Natl. Acad. Sci. USA*, 105, 10291-10296, doi:10.1073/pnas.0804860105,
901 2008.

902 Zhang, R. Y., Khalizov, A., Wang, L., Hu, M., and Xu, W.: Nucleation and Growth of
903 Nanoparticles in the Atmosphere, *Chem. Rev.*, 112, 1957-2011, doi:10.1021/Cr2001756,
904 2012.

905 Zuberi, B., Johnson, K. S., Aleks, G. K., Molina, L. T., and Laskin, A.: Hydrophilic properties of
906 aged soot, *Geophys. Res. Lett.*, 32, L01807, doi:10.1029/2004gl021496, 2005.

907

908 **Table 1.** BC physical properties used in theoretical calculations^a

Aging Stage ^b	Pure BC		Coating material		Standard calculation	Sensitivity calculation
	Mobility diameter (nm)	Mass (10 ⁻¹⁶ g)	Species	Mass (10 ⁻¹⁶ g)		
I	155	5.13	--	--	BC aggregates with a fractal dimension of 2.1, BC refractive index of 1.95 – 0.79 <i>i</i> , and 164/416/651 primary spherules with diameters of 15 nm for three experimental cases, respectively	(1) BC refractive index of 1.75 – 0.63 <i>i</i> ; (2) Fractal dimension of 2.5; (3) Primary spherule diameter of 20 nm; (4) Single volume-equivalent BC sphere
	245	13.0				
	320	20.3				
II	155	5.13	Sulfuric acid (H ₂ SO ₄)	3.67	Concentric core-shell coating structures with BC refractive index of 1.95 – 0.79 <i>i</i>	(1) BC refractive index of 1.75 – 0.63 <i>i</i> ; (2) Off-center core-shell structure; (3) Closed-cell structure; (4) Open-cell structure (5) Partially encapsulated structure (6) Externally attached structure
	245	13.0		11.0		
	320	20.3		17.9		
III	155	5.13	Sulfuric acid and water (H ₂ SO ₄ -H ₂ O)	7.59	Concentric core-shell coating structures with BC refractive index of 1.95 – 0.79 <i>i</i>	(1) BC refractive index of 1.75 – 0.63 <i>i</i> ; (2) Off-center core-shell structure; (3) Closed-cell structure; (4) Open-cell structure (5) Partially encapsulated structure (6) Externally attached structure
	245	13.0		20.7		
	320	20.3		33.6		

909 ^aParticle properties are derived from measurements in laboratory experiments (Zhang et al., 2008)
910 with initial BC mobility diameters of 155, 245 and 320 nm. See text for details.

911 ^b See Fig. 1 and text for details.

912

913

914 **Figure captions:**

915

916 **Figure 1.** A theoretical model that accounts for three BC aging stages and the associated BC
917 structures, including freshly emitted aggregates (Stage I), coated BC by soluble material (Stage
918 II), and those after further hygroscopic growth (Stage III). Six typical structures for coated BC at
919 Stages II and III are considered based on atmospheric observations, including embedded (i.e.,
920 concentric core-shell, off-center core-shell, and closed-cell), partially encapsulated, and partly
921 coated (i.e., open-cell and externally attached) structures. See text for details.

922

923 **Figure 2.** A graphical description of the geometric-optics surface-wave (GOS) approach for light
924 scattering and absorption by coated BC aggregates. The GOS components include the
925 hit-and-miss Monte Carlo photon tracing associated with internal and external refractions and
926 reflections, diffraction following Babinet's principle for randomly oriented irregular particles,
927 and surface waves travelling along the particle edges and propagating into shadow regions. See
928 text for details.

929

930 **Figure 3.** Laboratory measurements and theoretical calculations of BC extinction (left column),
931 absorption (middle column), and scattering (right column) cross sections (at 532 nm) at three
932 aging stages for BC with initial mobility diameters (D_{BC}) of 155 nm (top row), 245 nm (middle
933 row), and 320 nm (bottom row). Black circles represent mean values from measurements and
934 black error bars indicate experimental uncertainties reported by Zhang et al. (2008) and Khalizov
935 et al. (2009a). Green squares indicate results from the standard theoretical calculations (see Table
936 1 for details). Red crosses represent mean values for theoretical calculations using BC refractive
937 index of $1.95 - 0.79i$ and $1.75 - 0.63i$ and Red error bars indicate the range of theoretical
938 calculations using BC refractive index of $1.95 - 0.79i$ (upper bound) and $1.75 - 0.63i$ (lower
939 bound)the corresponding upper and lower bounds. Blue error bars represent the upper and lower
940 bounds of sensitivity calculations using different BC morphology with refractive index of $1.95 -$
941 $0.79i$ (see also Fig. 1 and Table 1).

942

943 **Figure 4.** Extinction (red), absorption (blue), and scattering (orange) cross sections (at 532 nm)
944 for different BC morphology normalized by BC aggregate cross sections determined from
945 standard calculations at aging Stage I for initial BC mobility diameters (D_{BC}) of 155 nm (top),
946 245 nm (middle), and 320 nm (bottom). Results for fFour BC structures are consideredshown,
947 including BC aggregates in standard calculations (circles) with a fractal dimension (D_f) of 2.1
948 and a primary spherule diameter (D_p) of 15 nm, BC aggregates with a fractal dimension (D_f) of
949 2.5 (triangles; vs-versus 2.1 in standard calculations), BC aggregates with a primary spherule
950 diameter (D_p) of 20 nm (squares; vs-versus 15 nm in standard calculations), and a single
951 mass-equivalent BC sphere (crosses; vs-versus fractal aggregate in standard calculations).
952 Dashed horizontal lines indicate a value of 1.

953

954 **Figure 5.** Extinction (red), absorption (blue), and scattering (orange) cross sections (at 532 nm)

955 for different coating morphology normalized by cross sections of concentric core-shell structures
956 determined from standard calculations at aging Stage II (BC coated by sulfuric acid (H_2SO_4)) for
957 initial BC mobility diameters (D_{BC}) of 155 nm (top), 245 nm (middle), and 320 nm (bottom). Six
958 BC coating structures are considered, including concentric core-shell (circles), off-center
959 core-shell (triangles), closed-cell (squares), open-cell (crosses), partly encapsulated (diamonds),
960 and externally attached (asterisks) structures (see also Fig. 1). Dashed horizontal lines indicate a
961 value of 1.

962

963 **Figure 6.** Same as Fig. 5, but for aging stage III where BC particles are coated by both sulfuric
964 acid and water ($H_2SO_4-H_2O$).

965

966 **Figure 7.** Enhancement in BC absorption (top) and scattering (bottom) during aging from freshly
967 emitted aggregates at Stage I to BC coated by sulfuric acid (H_2SO_4) at Stage II (circles) and by
968 both sulfuric acid and water ($H_2SO_4-H_2O$) at Stage III (crosses) for initial BC mobility sizes (D_{BC})
969 of 155 nm (left), 245 nm (middle), and 320 nm (right). The enhancements for different BC
970 coating morphology are shown, including concentric core-shell, off-center core-shell, closed-cell,
971 open-cell, partly encapsulated, and externally attached structures (~~See-see~~ also Fig. 1). The
972 reference case for enhancement calculation is the fresh BC aggregate measured in laboratory
973 experiments, which is used for all six BC coating morphology cases. Thus, tThe enhancement is
974 computed as the ratio of calculated absorption/scattering cross sections of coated BC particles to
975 the-measured-observed values of fresh BC aggregates. Also shown is the measured enhancement
976 from laboratory experiments (Obs.).Horizontal dashed lines indicate a value of 1.0.

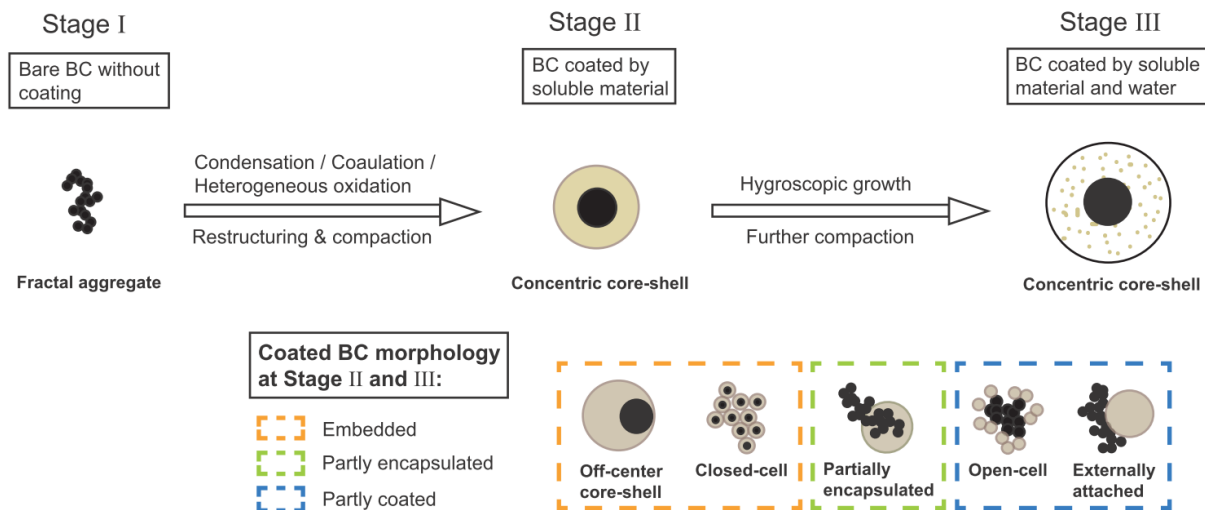
977

978 ~~**Figure 8.** Observations of (a) BC coating thickness in diameter, (b) fraction of coated BC, and (c)~~
979 ~~column BC loads, and model simulations of (d) effective BC mass absorption cross section~~
980 ~~(MAC), (e) effective BC single scattering albedo (SSA), and (f) BC direct radiative forcing~~
981 ~~(DRF) at the top of atmosphere over five regions (grey rectangles) during the CalNex 2010~~
982 ~~measurements, including (I) West LA Basin, (II) East LA Basin, (III) Banning Pass, (IV)~~
983 ~~Banning Outflow, and (V) Imperial Valley. Also shown are 1σ uncertainties (error bars) of~~
984 ~~observations in (a) (c) and the range (error bars) of model results using BC refractive index of~~
985 ~~$1.95 - 0.79i$ and $1.75 - 0.63i$ in (d) (f). Dashed grey lines in (d) (f) represent upper and lower~~
986 ~~bounds of model results using different BC morphology (see also Fig. 1 and Table 1) with~~
987 ~~refractive index of $1.95 - 0.79i$.~~

988

989

990

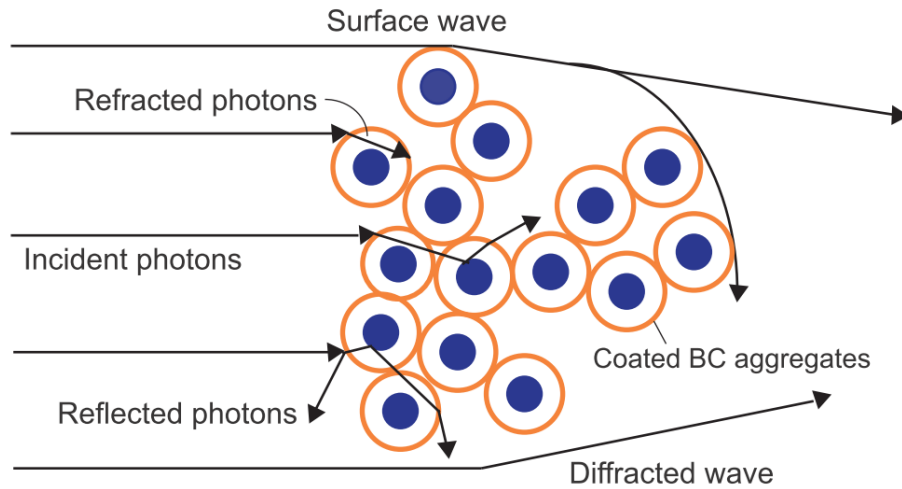


991

992

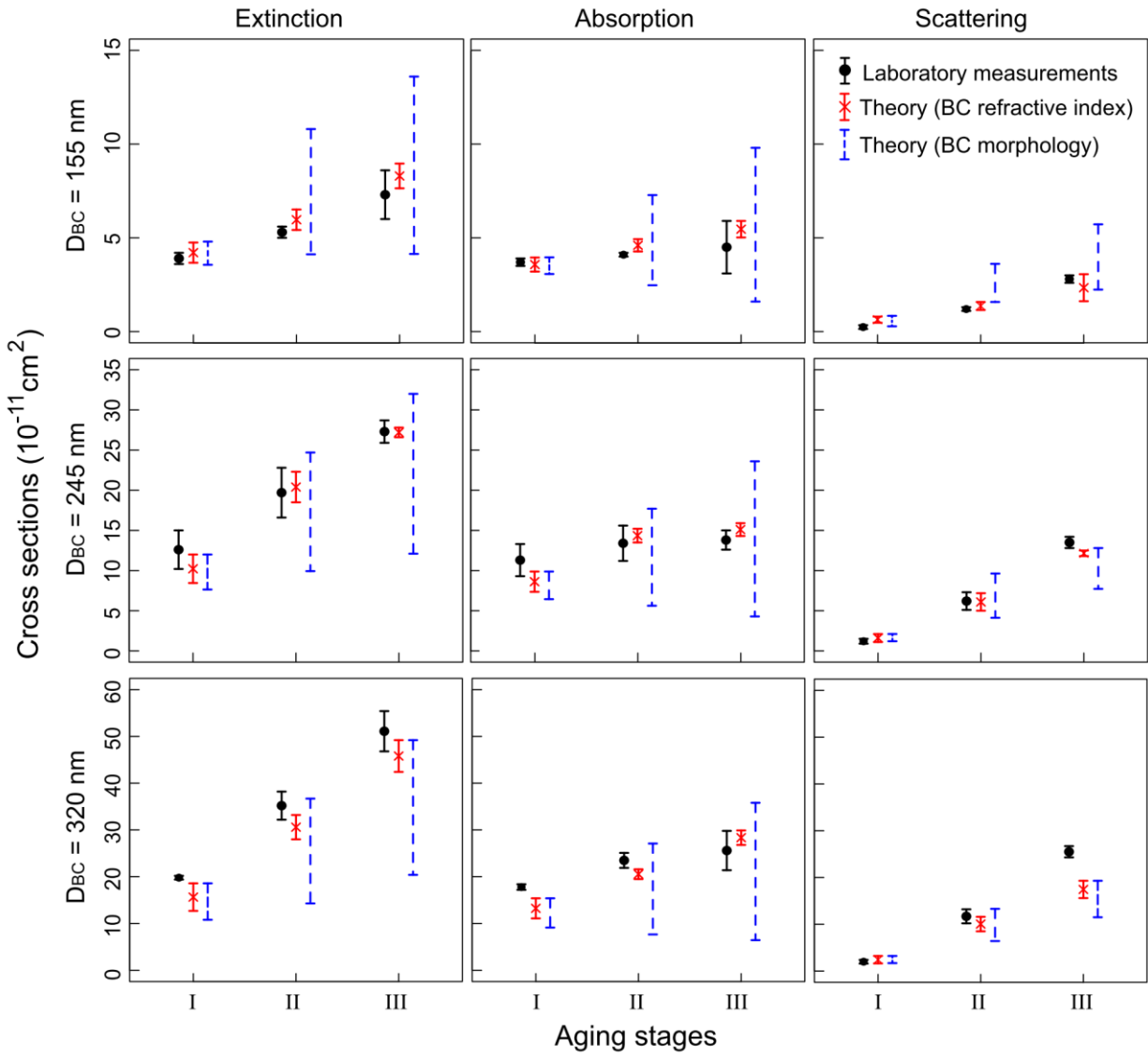
993 **Figure 1.** A theoretical model that accounts for three BC aging stages and the associated BC
 994 structures, including freshly emitted aggregates (Stage I), coated BC by soluble material (Stage
 995 II), and those after further hygroscopic growth (Stage III). Six typical structures for coated BC at
 996 Stages II and III are considered based on atmospheric observations, including embedded (i.e.,
 997 concentric core-shell, off-center core-shell, and closed-cell), partly encapsulated, and partly
 998 coated (i.e., open-cell and externally attached) structures. See text for details.

999

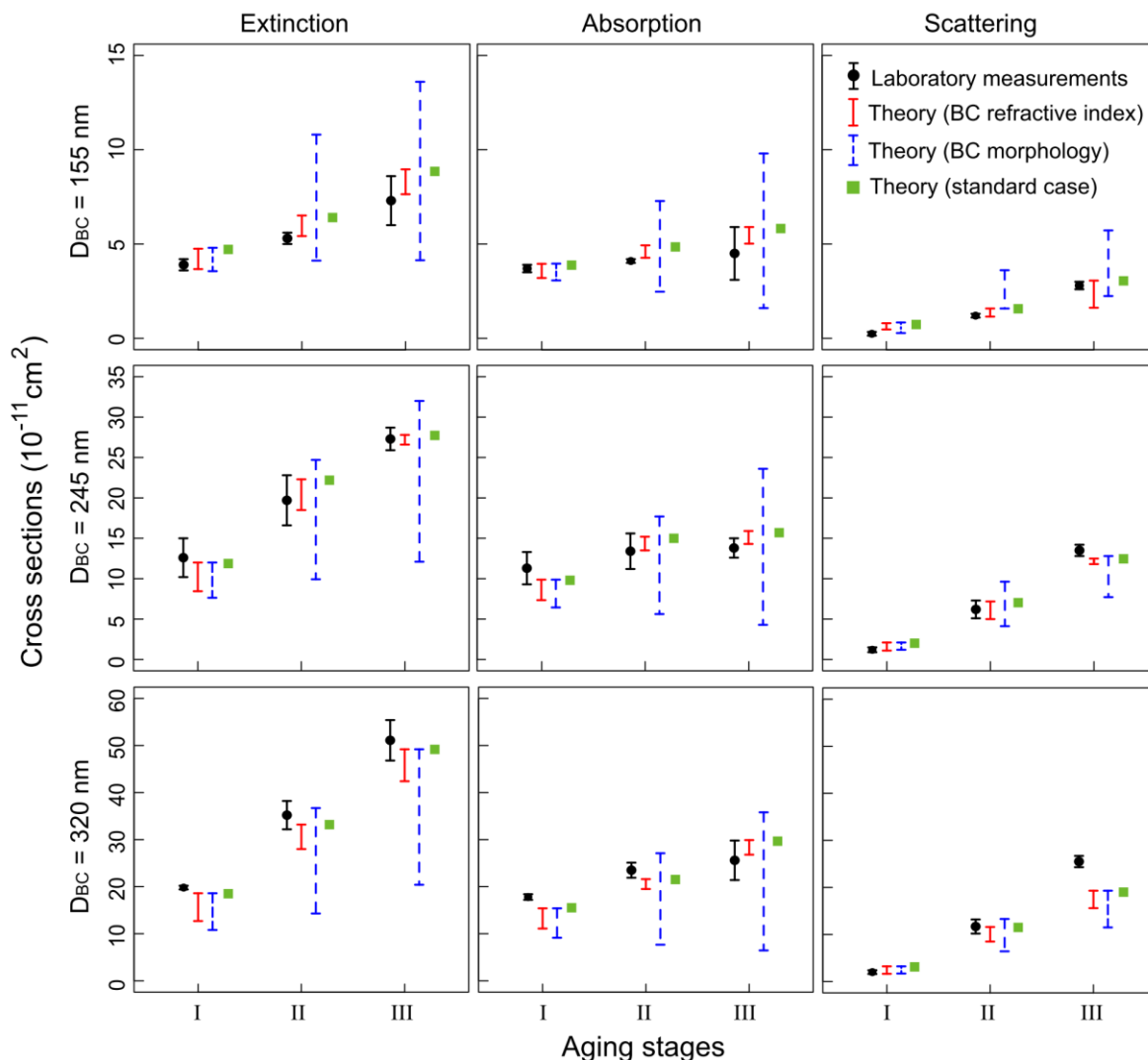


1000
 1001
 1002
 1003
 1004
 1005
 1006
 1007
 1008
 1009

Figure 2. A graphical description of the geometric-optics surface-wave (GOS) approach for light scattering and absorption by coated BC aggregates. The GOS components include the hit-and-miss Monte Carlo photon tracing associated with internal and external refractions and reflections, diffraction following Babinet’s principle for randomly oriented irregular particles, and surface waves travelling along the particle edges and propagating into shadow regions. See text for details.



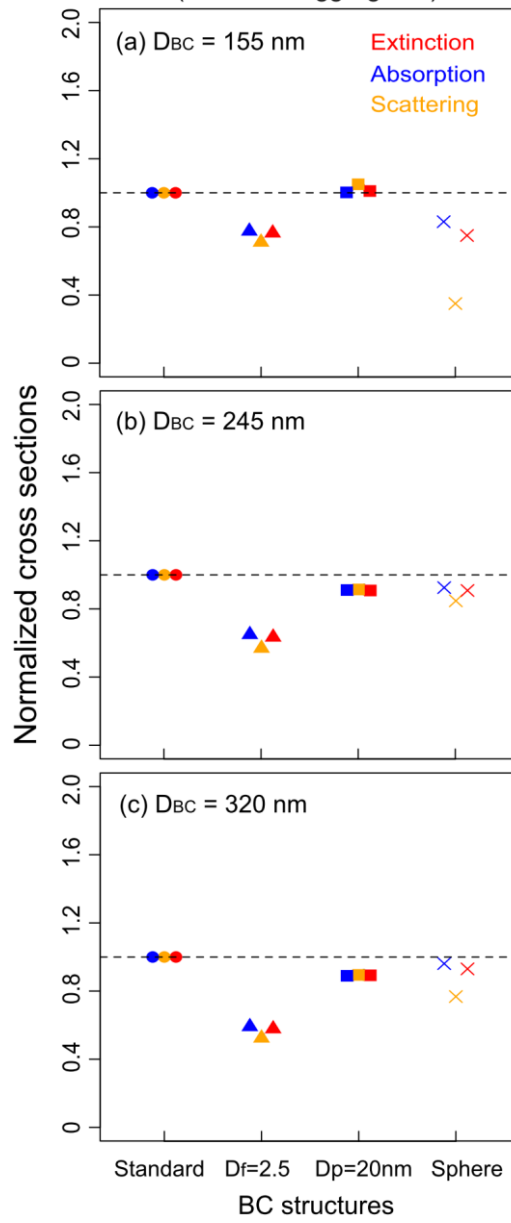
1010

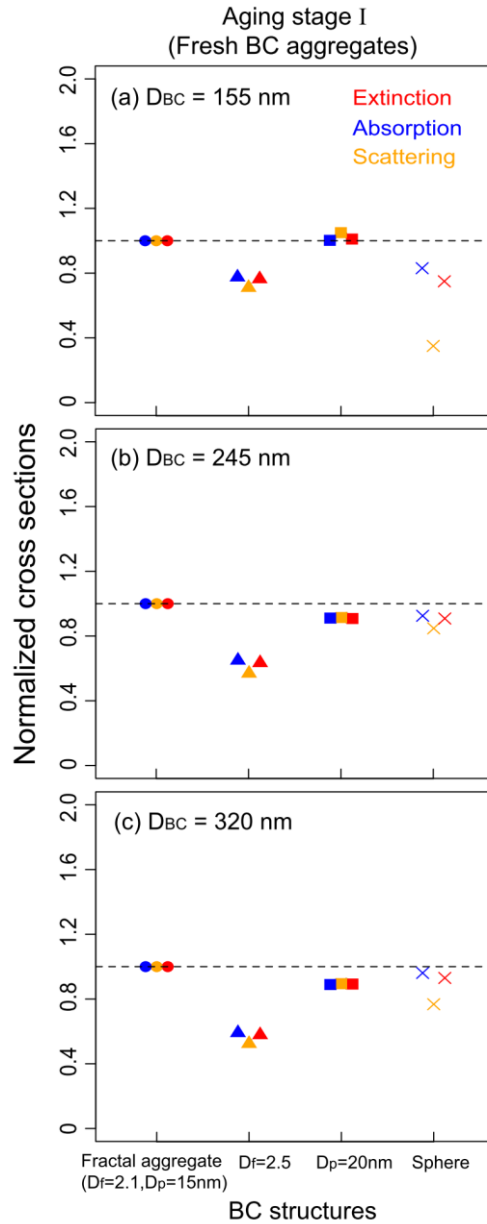


1011
 1012
 1013
 1014
 1015
 1016
 1017
 1018
 1019
 1020
 1021
 1022
 1023
 1024
 1025
 1026

Figure 3. Laboratory measurements and theoretical calculations of BC extinction (left column), absorption (middle column), and scattering (right column) cross sections (at 532 nm) at three aging stages for BC with initial mobility diameters (D_{BC}) of 155 nm (top row), 245 nm (middle row), and 320 nm (bottom row). Black circles represent mean values from measurements and black error bars indicate experimental uncertainties reported by Zhang et al. (2008) and Khalizov et al. (2009a). Green squares indicate results from the standard theoretical calculations (see Table 1 for details). Red crosses represent mean values for theoretical calculations using BC refractive index of $1.95 - 0.79i$ and $1.75 - 0.63i$ and red error bars indicate the range of theoretical calculations using BC refractive index of $1.95 - 0.79i$ (upper bound) and $1.75 - 0.63i$ (lower bound) the corresponding upper and lower bounds. Blue error bars represent the upper and lower bounds of sensitivity calculations using different BC morphology with refractive index of $1.95 - 0.79i$ (see also Fig. 1 and Table 1).

Aging stage I
(Fresh BC aggregates)

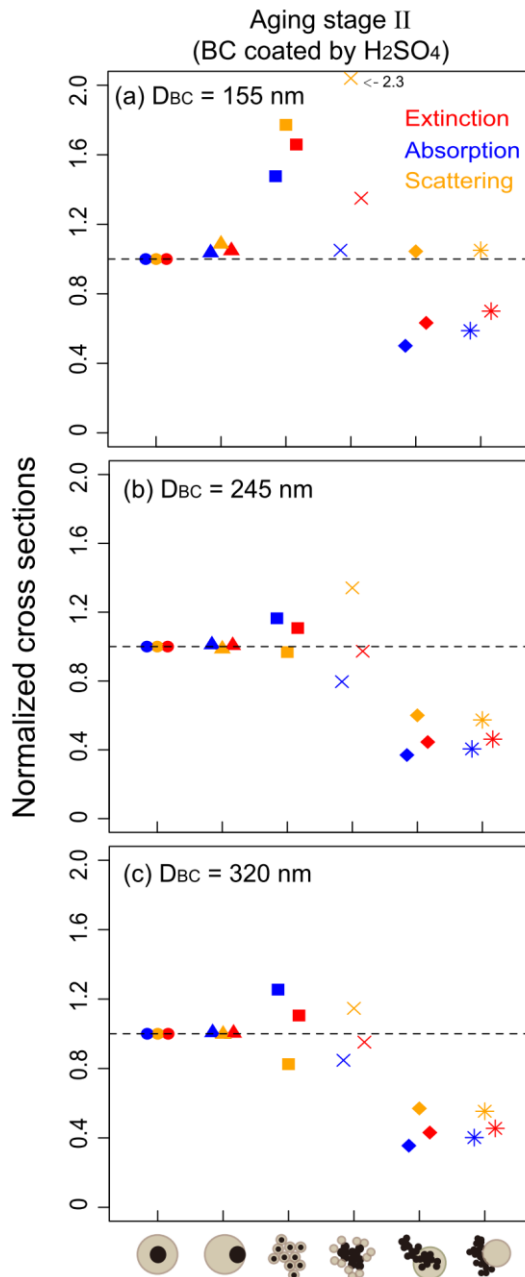




1028

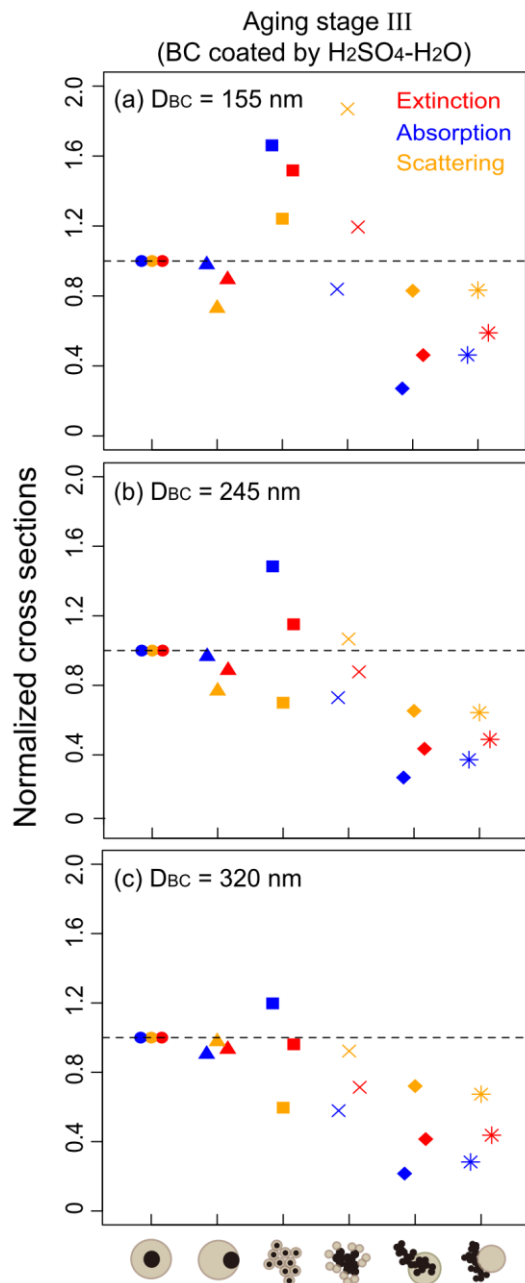
1029

1030 **Figure 4.** Extinction (red), absorption (blue), and scattering (orange) cross sections (at 532 nm)
 1031 for different BC morphology normalized by BC aggregate cross sections determined from
 1032 standard calculations at aging Stage I for initial BC mobility diameters (D_{BC}) of 155 nm (top),
 1033 245 nm (middle), and 320 nm (bottom). Results for four BC structures are considered shown,
 1034 including BC aggregates in standard calculations (circles) with a fractal dimension (D_f) of 2.1
 1035 and a primary spherule diameter (D_p) of 15 nm, BC aggregates with a fractal dimension (D_f) of
 1036 2.5 (triangles; vs. versus 2.1 in standard calculations), BC aggregates with a primary spherule
 1037 diameter (D_p) of 20 nm (squares; vs. versus 15 nm in standard calculations), and a single
 1038 mass-equivalent BC sphere (crosses; vs. versus fractal aggregate in standard calculations).
 1039 Dashed horizontal lines indicate a value of 1.



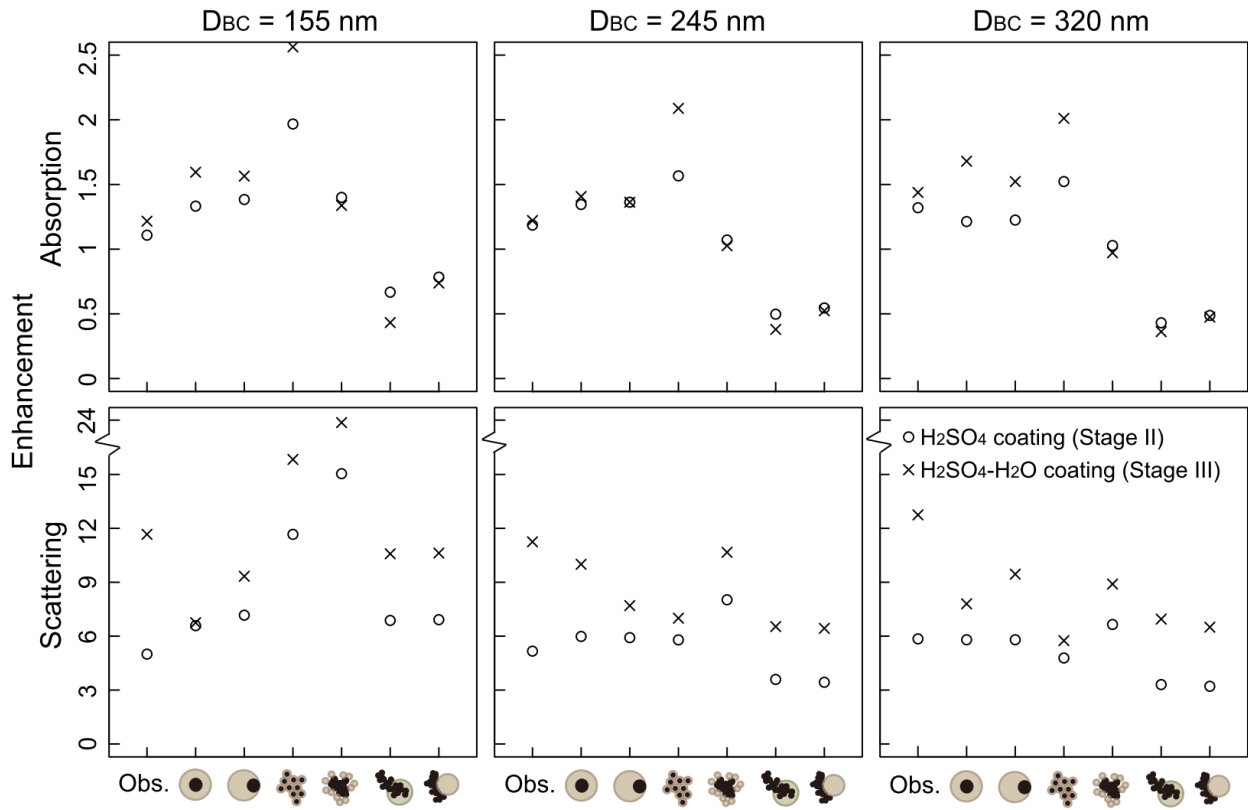
1040
1041
1042
1043
1044
1045
1046
1047
1048
1049
1050

Figure 5. Extinction (red), absorption (blue), and scattering (orange) cross sections (at 532 nm) for different coating morphology normalized by cross sections of concentric core-shell structures determined from standard calculations at aging Stage II (BC coated by sulfuric acid (H₂SO₄)) for initial BC mobility diameters (D_{BC}) of 155 nm (top), 245 nm (middle), and 320 nm (bottom). Six BC coating structures are considered, including concentric core-shell (circles), off-center core-shell (triangles), closed-cell (squares), open-cell (crosses), partly encapsulated (diamonds), and externally attached (asterisks) structures (see also Fig. 1). Dashed horizontal lines indicate a value of 1.



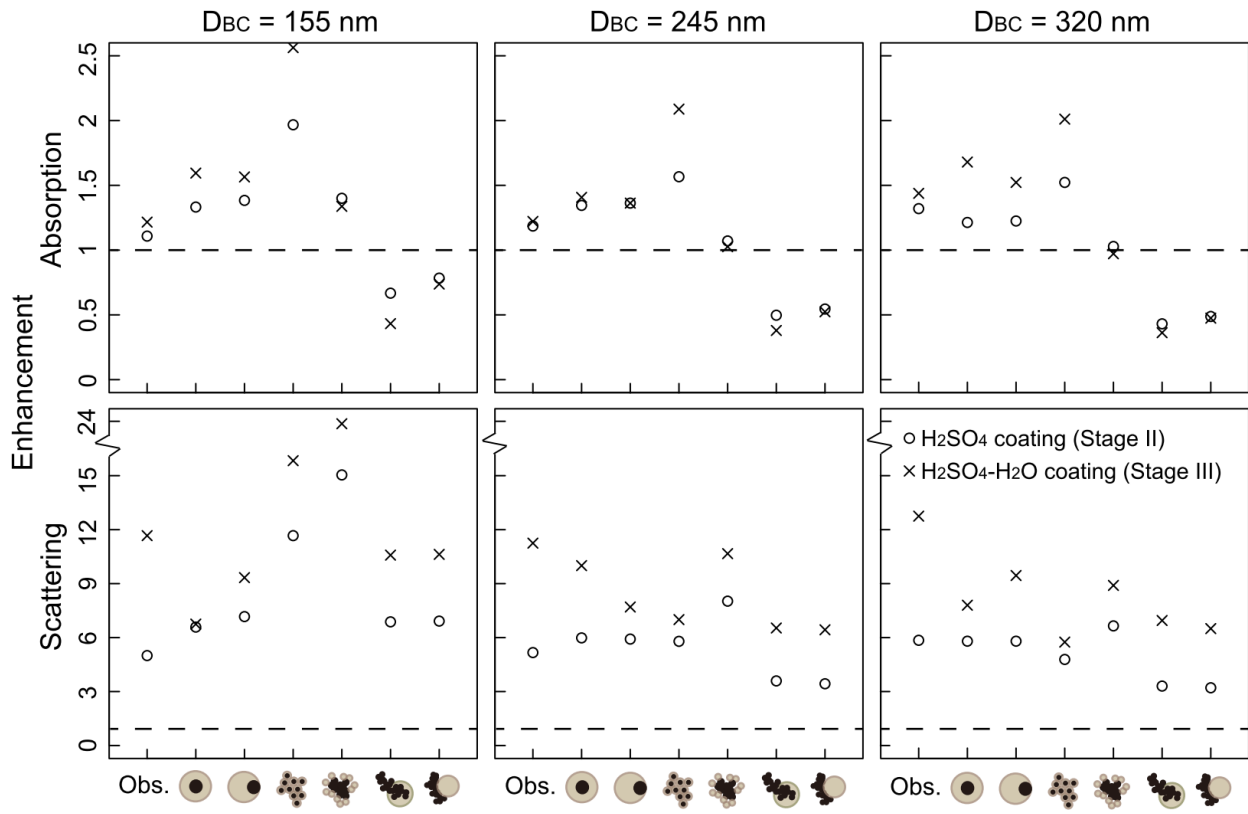
1051
1052
1053
1054
1055

Figure 6. Same as Fig. 5, but for aging stage III where BC particles are coated by both sulfuric acid and water (H₂SO₄-H₂O).



1056

1057



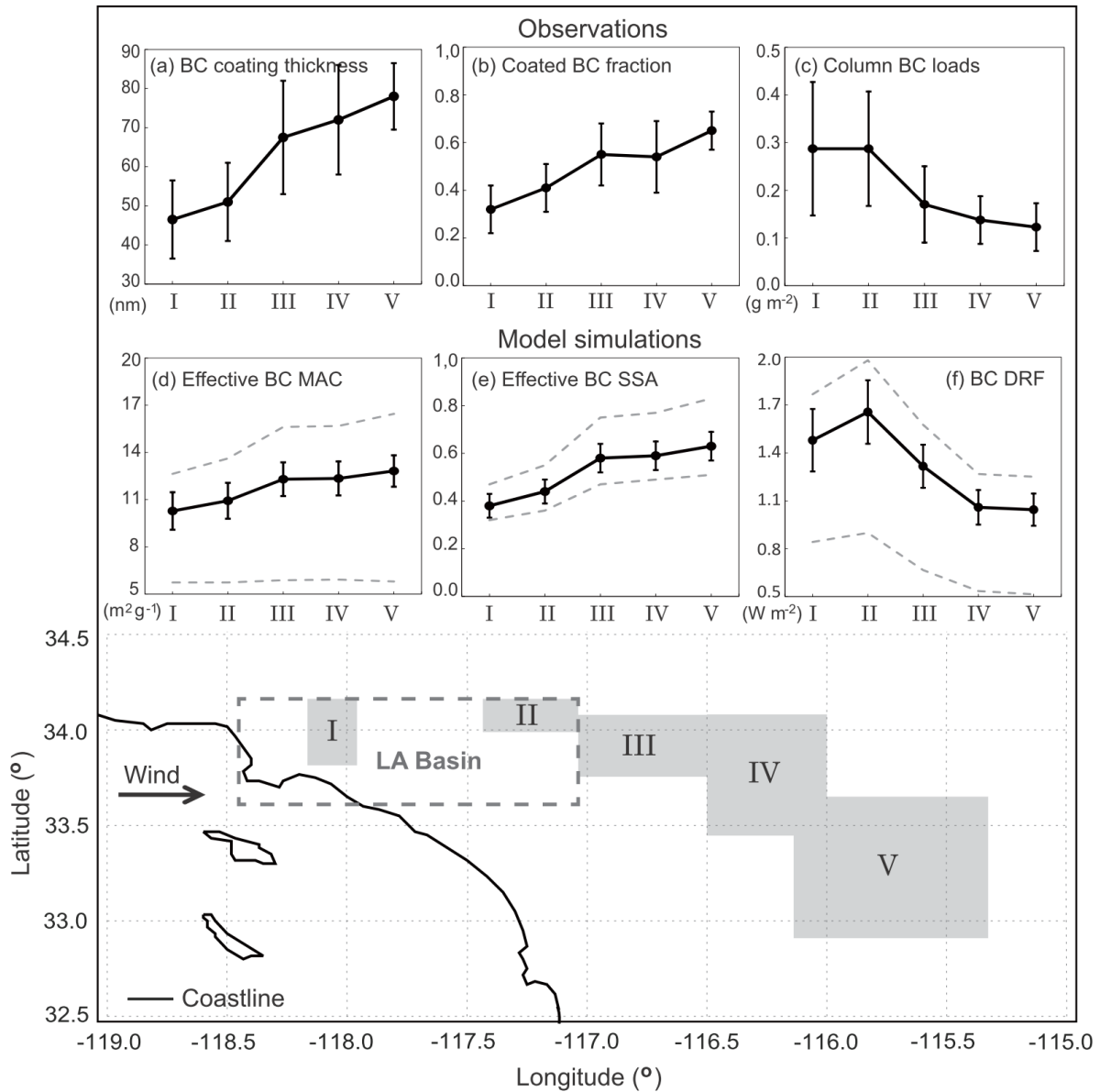
1058

1059

1060 **Figure 7.** Enhancement in BC absorption (top) and scattering (bottom) during aging from freshly
 1061 emitted aggregates at Stage I to BC coated by sulfuric acid (H₂SO₄) at Stage II (circles) and by
 1062 both sulfuric acid and water (H₂SO₄-H₂O) at Stage III (crosses) for initial BC mobility sizes (D_{BC})
 1063 of 155 nm (left), 245 nm (middle), and 320 nm (right). The enhancements for different BC
 1064 coating morphology are shown, including concentric core-shell, off-center core-shell, closed-cell,
 1065 open-cell, partly encapsulated, and externally attached structures (See-see also Fig. 1). The
 1066 reference case for enhancement calculation is the fresh BC aggregate measured in laboratory
 1067 experiments, which is used for all six BC coating morphology cases. Thus, the enhancement is
 1068 computed as the ratio of calculated absorption/scattering cross sections of coated BC particles to
 1069 the measured-observed values of fresh BC aggregates. Also shown is the measured enhancement
 1070 from laboratory experiments (Obs.).Horizontal dashed lines indicate a value of 1.0.

1071

1072



1073
1074
1075
1076
1077
1078
1079
1080
1081
1082
1083
1084

Figure 8. Observations of (a) BC coating thickness in diameter, (b) fraction of coated BC, and (c) column BC loads, and model simulations of (d) effective BC mass absorption cross section (MAC), (e) effective BC single scattering albedo (SSA), and (f) BC direct radiative forcing (DRF) at the top-of-atmosphere over five regions (grey rectangles) during the CalNex 2010 measurements, including (I) West LA Basin, (II) East LA Basin, (III) Banning Pass, (IV) Banning Outflow, and (V) Imperial Valley. Also shown are 1σ uncertainties (error bars) of observations in (a)–(c) and the range (error bars) of model results using BC refractive index of $1.95 - 0.79i$ and $1.75 - 0.63i$ in (d)–(f). Dashed grey lines in (d)–(f) represent upper and lower bounds of model results using different BC morphology (see also Fig. 1 and Table 1) with refractive index of $1.95 - 0.79i$.